Indirect aerosol forcing in a climate model with an interactive sulphur cycle.

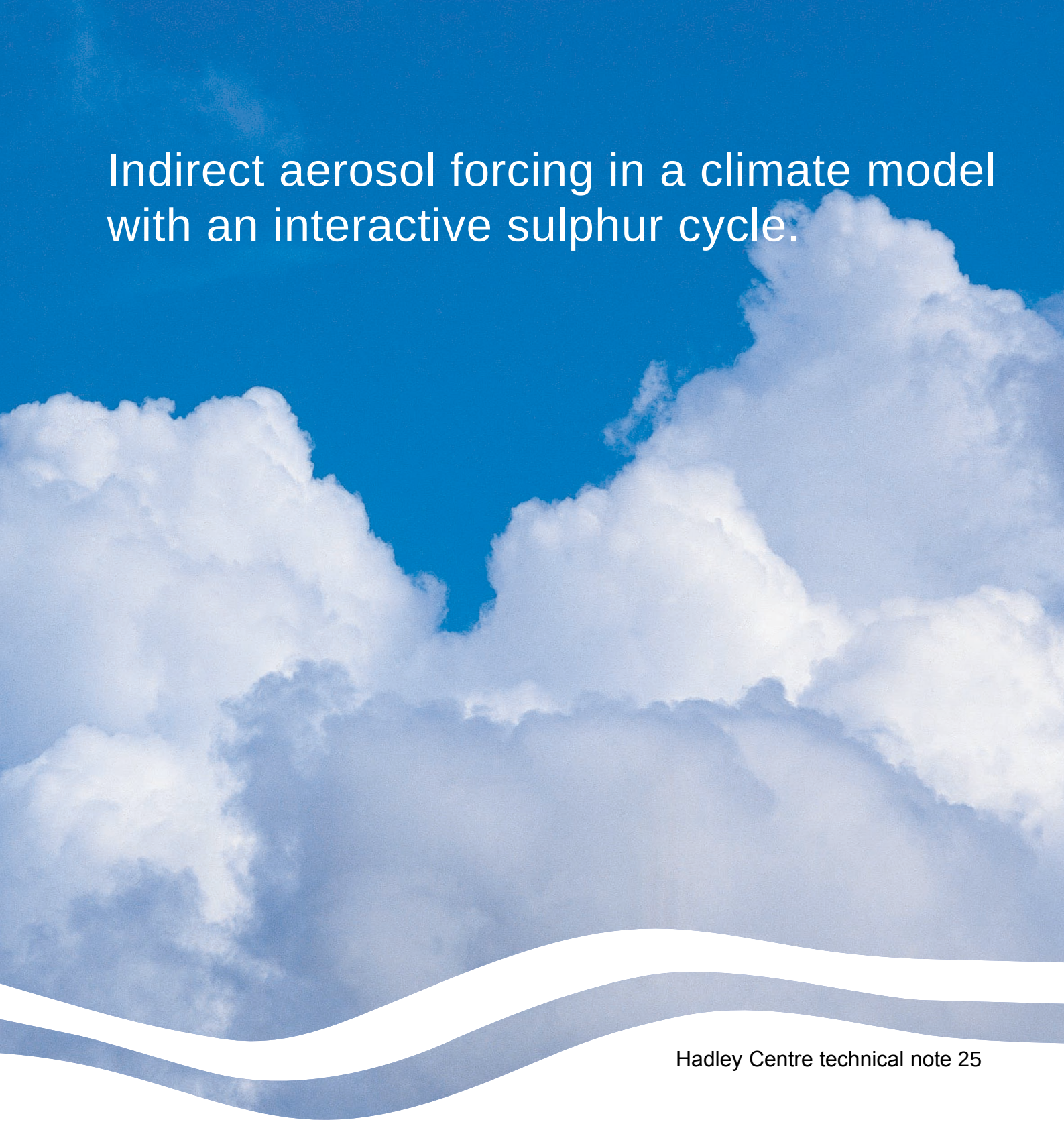

Hadley Centre technical note 25

Andy Jones, David L. Roberts,
Margaret J. Woodage and Colin E. Johnson

February 2001

Met Office

Indirect aerosol forcing in a climate model with an interactive sulphur cycle

Andy Jones, David L. Roberts, Margaret J. Woodage
and Colin E. Johnson

Hadley Centre for Climate Prediction and Research
The Met. Office
London Road
Bracknell
RG12 2SY
UK

Email: ajones@meto.gov.uk

Short title: Indirect aerosol forcing

Abstract. The effects of anthropogenic sulphate aerosol on cloud albedo and on precipitation efficiency (the first and second indirect effects respectively) are investigated using a new version of the Hadley Centre climate model. This version includes a new cloud microphysics scheme, an interactive sulphur cycle and a parametrization of the effects of sea-salt aerosol. The combined global mean radiative impact from both indirect effects is estimated to be approximately -1.9 Wm^{-2} in terms of the change in net cloud forcing, with the 'albedo' effect dominating. This estimate has at least a factor of 2 uncertainty associated with it: for example, alternative assumptions which affect the concentration of natural 'background' sulphate aerosol reduce the forcing by over 25%, and different parametrizations of the autoconversion of cloud droplets to rainwater can double the forcing.

1. Introduction

The impact of anthropogenic sulphate aerosol on the Earth's radiation budget may be divided into direct and indirect effects. The former involves the direct scattering or absorption of incoming solar radiation by the aerosol particles. The latter concerns the effects of aerosol particles on clouds. The direct effect has been estimated to exert a negative (cooling) radiative forcing on the climate system in the range -0.2 to -0.8 Wm^{-2}, which is significant when compared with the estimated positive (warming) forcing of $+2.5$ Wm^{-2} from increases in greenhouse gases to date (all estimates *IPCC* 1996). The indirect effects of aerosols operate by increasing the number concentration of cloud condensation nuclei (CCN), so increasing the concentration of cloud droplets and thereby (assuming constant cloud water content) reducing the mean size of cloud droplets (*Twomey* 1974). This reduction in cloud droplet size has two further effects: firstly, clouds with smaller droplets reflect more solar radiation back to space; this first indirect effect is sometimes known as the 'albedo' effect. Previous work has estimated this effect to be in the range -0.5 to -1.5 Wm^{-2} (*e.g. Boucher and Lohmann* 1995, *Jones and Slingo* 1996). Secondly, the reduction in cloud droplet size also affects the efficiency with which clouds form precipitation, tending to increase the amount of water in clouds and also affecting their persistence. Consequently, this second indirect effect (sometimes known as the 'lifetime' effect), as well as having a cooling effect in the shortwave due to the clouds being brighter, could also exert a longwave warming influence due to the increase in cloud water.

The early stages of cloud droplet growth occur by the condensation of water vapour onto CCN once the relative humidity just exceeds 100%. However, the rate of condensational growth slows as the droplets become larger, and this process alone cannot account for the formation of precipitation-sized particles in warm clouds in the times observed (*e.g. Pruppacher and Klett* 1997). Precipitation production in non-freezing clouds depends on the runaway growth of a small fraction of cloud droplets which become large enough to fall with appreciable speeds relative to the other cloud droplets, so colliding and coalescing with them and thereby growing larger. The process of precipitation formation by this collision-coalescence mechanism is referred to as the autoconversion of cloud water to rainwater. For the same cloud water content, autoconversion is slower for a high concentration of smaller droplets than for a low concentration of larger droplets. This is because smaller droplets have lower relative fallspeeds, tend to flow around one another rather than colliding and coalescing, and also require more collisions to reach raindrop size; this is the basis of the 'lifetime' effect.

Albrecht [1989] proposed that increases in CCN could decrease the formation rate of drizzle in marine stratiform clouds. This would reduce the rate at which the cloud water was dissipated, so increasing the lifetime of the cloud and thereby exerting a cooling effect by the increased persistence of reflective clouds. Experimental studies over the eastern Pacific of the effects of aerosols from ship exhausts on clouds support the validity of this mechanism (*Durkee et al.* 2000; *Ferek et al.* 2000). Over the Atlantic, measurements of clean and polluted clouds have found a relative dearth of drizzle drops in polluted clouds (*Hudson and Li* 1995). The mechanism is also supported by detailed cloud/boundary-layer models (*Ackerman et al.* 1995). General circulation model (GCM) studies of both indirect effects (*Lohmann and Feichter* 1997, *Rotstayn* 1999, *Lohmann et al.* 2000) have found the second effect to be of comparable magnitude to the first, indicating that account should be taken of it in modelling recent and future climate change.

In this study we use a newly-developed interactive sulphur cycle scheme and a new microphysics scheme to estimate the impact of the first and second indirect effects in the Hadley Centre GCM. In addition to modelling sulphate aerosol, this study also includes a parametrization of the effects of sea-salt aerosol. The climate model and details of modelling the indirect effects are presented in Sections 2 and 3. The sulphur cycle is described in Section 4, the general design and rationale of the experiments in Section 5, and the results

presented in Section 6. Finally, discussion of these results and some conclusions are presented in Section 7.

2. The Climate Model

The model used in this study is based on HadAM4 (*Webb et al.* 2000). This is a development of the previous HadAM3 model (*Pope et al.* 2000) and is a configuration of the atmospheric component of the Met. Office's Unified Model (*Cullen* 1993). The model has a horizontal resolution of 2.5° latitude by 3.75° longitude with 38 levels in the vertical (defined in Appendix A); it was run with a timestep of 30 minutes using climatological sea-surface temperatures as a boundary condition. One of the main improvements over HadAM3 is a new mixed-phase precipitation scheme (*Wilson and Ballard* 1999). The cloud scheme is based on that of *Smith* [1990] but introduces a new prognostic variable for cloud ice. Calculation of the exchanges between ice, liquid and vapour is done using physically-based transfer terms, which is an improvement on previous schemes where the partitioning between liquid- and ice-phase cloud was diagnosed purely as a function of temperature. Further improvements include the treatment of the radiative effects of anvil cirrus (*Gregory* 1999) and a parametrization of the radiative effects of non-spherical cloud ice particles (*Kristjánsson et al.* 1999). A parametrization of cloud amount which allows clouds to fill only part of the vertical thickness of a model gridbox has been introduced, and also a parametrization of the threshold relative humidity for cloud formation in terms of the horizontal variability resolved by the climate model (*Cusack et al.* 1999).

An important addition to HadAM4 in the version used here is the inclusion of a prognostic sulphur-cycle scheme. This allows the model to calculate the distribution of sulphate aerosol mass concentration interactively, as opposed to using fixed time-mean fields of sulphate calculated in separate experiments as employed previously (*e.g. Jones and Slingo* 1996). This new scheme is outlined in Section 4 below.

Cloud droplet effective radii (r_e) for stratiform and shallow convective clouds are calculated using the parametrization of *Martin et al.* [1994]:

$$r_e = \sqrt[3]{\frac{3\, q_c\, \rho_o}{4\pi\, \rho_w\, \mathrm{k}\, N_d}}\,. \tag{1}$$

q_c is the cloud liquid water content (kg kg^{-1}), ρ_o and ρ_w the densities of air and water, and N_d is the cloud droplet number concentration. The value of k depends on whether the clouds are continental or maritime (taken as whether over land or sea in the model) — see *Martin et al.* for details. For deep convective clouds the constant values suggested by *Bower et al.* [1994] are used. The characteristic particle size for cloud ice crystals is calculated using the parametrization of *Kristjánsson et al.* [1999]. This parametrization depends only on temperature and so there is no contribution from the ice-phase to the indirect effects modelled here. Below 0°C clouds are separated into adjacent liquid and ice regions for radiative purposes, the relative sizes of the regions depending on the cloud liquid- and ice-water contents.

Experiments concerning the indirect effects of aerosols obviously require that cloud droplet concentrations are determined from aerosol concentrations. In the model used here N_d depends on three factors:

2.1. Sulphate

Although it is now well established that sulphate does not dominate aerosol composition as much as once thought (*e.g. Rivera-Carpio et al.* 1996, *Hegg et al.* 1997, *Murphy et al.*

1998), it is nevertheless still an important component of the atmospheric aerosol. In the model the number concentration of sulphate aerosol particles is calculated from the mass concentration of aerosol sulphur predicted by the internal sulphur-cycle scheme (see Section 4) using the same assumptions as *Jones et al.* [1994]. This reduces to:

$$A_{\mathrm{SO_4}} = 5.125 \times 10^{17}\, m \tag{2}$$

where $A_{\mathrm{SO_4}}$ is the number of ammonium sulphate aerosol particles ($\mathrm{m^{-3}}$) and m is the total mass concentration of aerosol sulphur ($\mathrm{kg\ m^{-3}}$).

2.2. Sea-salt

Observations have shown that sea-salt can be an important source of CCN in the marine environment (*e.g. O'Dowd and Smith* 1993, *Murphy et al.* 1998). Consequently a simple diagnostic treatment of sea-salt aerosol number concentration was included in the model. Over the sea the number concentration of sea-salt particles was calculated as a function of 10m windspeed (u) using parametrizations based on observational data (*O'Dowd et al.* 1997, 1999):

$0\ \mathrm{ms^{-1}} \leq u \leq 2\ \mathrm{ms^{-1}}$:

$$A_f = 3.856 \times 10^6 (1 - e^{-0.736u}) \tag{3a}$$

$$A_j = 0.671 \times 10^6 (1 - e^{-1.351u}) \tag{3b}$$

$2\ \mathrm{ms^{-1}} \leq u \leq 17.5\ \mathrm{ms^{-1}}$:

$$A_f = 10^{(0.095u + 6.283)} \tag{3c}$$

$$A_j = 10^{(0.0422u + 5.7122)} \tag{3d}$$

$u > 17.5\ \mathrm{ms^{-1}}$:

$$A_f = 1.5 \times 10^8 (1 - 97.874 e^{-0.313u}) \tag{3e}$$

$$A_j = 3.6 \times 10^6 (1 - 103.926 e^{-0.353u}) \tag{3f}$$

where A_f and A_j are the number concentrations ($\mathrm{m^{-3}}$) of sea-salt aerosol particles originating from film and jet droplets respectively, the number concentration being dominated by the sub-micron film particles (see *O'Dowd et al.* 1999 for details). Following evidence from flights by the Met. Research Flight's C-130 aircraft, A_f and A_j were reduced exponentially with height with a scale height of 900m (*S. Osborne, pers. comm.*). At higher levels and over land these quantities are set to zero. As we are currently unable to take account of the size-related properties of sea-salt aerosols (aside from the different formation mechanisms implicit in Eqs. 3), only the total number of sea-salt aerosol particles is used in determining N_d.

The cloud droplet number concentration is determined using the relation of *Jones et al.* [1994] assuming an external mixture of sulphate and sea-salt:

$$N_d = \max\{3.75 \times 10^8 (1 - e^{-2.5 \times 10^{-9} A}), \mathrm{N_{min}}\} \tag{4}$$

where $A = A_{\mathrm{SO_4}} + A_f + A_j$ and $\mathrm{N_{min}} = 5 \times 10^6 \mathrm{m^{-3}}$ (but see Section 2.3 below).

2.3. Natural Continental CCN

Satellite retrievals of cloud droplet effective radii show a consistent tendency for r_e to be smaller over land than over the ocean (*Han et al.* 1994, *Kawamoto* 1999). In certain

areas this difference is due to anthropogenic aerosol sources, but the ubiquity of the land-sea difference suggests that this is not always the only cause. That it might be caused by systematically lower cloud water contents over land is discussed and rejected by *Jones and Slingo* [1996]. Therefore this difference in r_e is plausibly assumed to be at least partially due to naturally-occurring continental sources of CCN (*e.g.* organic aerosols, dust). In the model a crude attempt is made to take some account of this by increasing the minimum droplet concentration $\mathrm{N_{min}}$ over ice-free land from 5.0×10^6 to $3.5 \times 10^7 \mathrm{m}^{-3}$.

3. Modelling the Indirect Effects of Aerosols

3.1. The First Indirect Effect

The first indirect effect is modelled by using equations (1)–(4), *i.e.* by allowing the cloud droplet effective radius used in the radiation scheme to be calculated using a variable N_d dependent on aerosol concentration.

3.2. The Second Indirect Effect

As discussed in the introduction, the key process for the second indirect effect is the autoconversion of cloudwater to rainwater. The autoconversion parametrization of the new precipitation scheme (*Wilson and Ballard* 1999) is based on that of *Tripoli and Cotton* [1980], and can be thought of as consisting of a 'rate' part and a 'threshold' part. The rate of increase of the mass mixing ratio of rainwater by autoconversion from cloudwater, R_{auto}, is given by:

$$R_{auto} = \frac{0.104\ \mathrm{g}\ \mathrm{E_c}\ \rho_o^{\frac{4}{3}}}{\mu\ \rho_w^{\frac{1}{3}}} \frac{q_c^{\frac{7}{3}}}{N_d^{\frac{1}{3}}} \tag{5}$$

where g is the acceleration due to gravity, $\mathrm{E_c}$ the collision/collection efficiency of cloud droplets (assumed to be 0.55, *Tripoli and Cotton* 1980) and μ the dynamic viscosity of air.

Autoconversion is allowed to proceed once q_c exceeds a threshold value $\mathrm{q_{min}}$. The value of $\mathrm{q_{min}}$ is used as a 'tunable' parameter in the standard precipitation scheme, but estimates of the second indirect effect can be sensitive to this threshold (*Fowler and Randall* 1996, *Rotstayn* 1999). We therefore also allow $\mathrm{q_{min}}$ to depend on aerosol concentration. *Rogers and Yau* [1989] suggest that autoconversion will only proceed once the number concentration of cloud droplets greater than 20μm in radius exceeds approximately 10^3 m^{-3}. Therefore, following *Pruppacher and Klett* [1997], a modified gamma cloud droplet size distribution is assumed, whereby knowledge of q_c and N_d allows the number concentration of large cloud droplets to be calculated. If this is greater than 10^3 m^{-3} then autoconversion is allowed to proceed. Consequently N_d, and therefore aerosol concentration, has a double impact on autoconversion: high values not only suppress R_{auto} *via* Eq. (5), they also increase the autoconversion threshold.

4. The Sulphur Cycle Model

Extra prognostic variables are required to simulate the distribution of sulphate aerosol. The present scheme involves five variables representing the mass mixing ratios of sulphur dioxide (SO_2), dimethyl sulphide (DMS) and three modes of sulphate. The latter comprise two size modes of free particle, labelled Aitken and accumulation modes, and a third mode

representing sulphate dissolved in cloud droplets. The free particle modes are assumed to have lognormal size distributions with parameters based on data reported by *Quinn et al.* [1995]: the Aitken mode has median radius 24 nm and geometric standard deviation 1.45; the corresponding parameters of the accumulation mode are 95 nm and 1.4. The three modes of sulphate reflect divisions observed in the real atmosphere (*e.g.* by *Hoppel et al.* 1990), and are represented explicitly in order to model their chemical and physical interactions more realistically. For example, the Aitken mode is produced by gas-phase oxidation of SO_2, while the accumulation mode is largely the result of cloud processing (*via* the dissolved mode). Treating the two free modes separately allows size-dependent processes to be represented better, for example in allowing differential rates of dry deposition. Large-scale vertical and horizontal advection of each variable is handled by the model's tracer advection scheme, which uses the flux redistribution method of *Roe* [1985] to maintain positive definiteness. Vertical transport by convection and turbulent mixing in the boundary layer are also parametrized in ways similar to the model's treatment of the vertical transport of heat and moisture.

The conversion of DMS to SO_2, and of SO_2 to sulphate, requires the parametrization of complex chemistry that is not yet completely understood. The approach taken here is fairly simple. Monthly average three-dimensional fields of the hydroxyl radical (OH), hydrogen peroxide (H_2O_2), the peroxide radical (HO_2) and ozone (O_3), produced from simulations using the Lagrangian chemistry model STOCHEM (*Collins et al.* 1997, *Stevenson et al.* 1997), are interpolated in space and time to provide boundary conditions that are used to control the rates of oxidation of DMS and SO_2. Details of the reactions are covered in the next two sub-sections.

4.1. DMS Oxidation

The parametrization of DMS oxidation has been constructed assuming that: (a) DMS reacts only with OH, ignoring its reaction with NO_3 and other species, and (b) the lifetimes of species intermediate between DMS and the final products are insignificant, *i.e.* the distribution of the final products depends only on DMS and oxidant concentrations. The validity of these assumptions will be discussed below. Note that two independent reactions of DMS with OH are permitted, representing the *addition* and *abstraction* pathways. The species intermediate between DMS and CH_3SO_2 are omitted, and the reactions of the latter species with NO_2 and HO_2 are neglected. The essence of the scheme is contained in the following set of reactions, the rate coefficients of which can be found in Table 1; M represents an air molecule.

$$\mathrm{DMS + OH \xrightarrow{k_1} CH_3SO_2} \tag{6}$$

$$\mathrm{DMS + OH \xrightarrow{0.9\,k_2} CH_3SO_2} \tag{7}$$

$$\mathrm{DMS + OH \xrightarrow{0.1\,k_2} MSA} \tag{8}$$

$$\mathrm{CH_3SO_2 + M \xrightarrow{k_3} SO_2 + CH_3 + M} \tag{9}$$

$$\mathrm{CH_3SO_2 + O_3 \xrightarrow{k_4} CH_3SO_3 + O_2} \tag{10}$$

$$\mathrm{CH_3SO_3 + HO_2 \xrightarrow{k_5} MSA + O_2} \tag{11}$$

$$\mathrm{CH_3SO_3 + M \xrightarrow{k_6} SO_3 + CH_3 + M} \tag{12}$$

In practice, this reaction set is implemented without explicitly storing the amounts of CH_3SO_2 and CH_3SO_3 as model variables. Instead, the rate coefficients are used to compute the relative importance of the various branches and thus the proportions of the three final products, MSA, SO_2 and SO_3. Of these, the MSA plays no further role in the model and is therefore effectively a sink of sulphur, while the SO_3 is assumed to be instantaneously converted to sulphate aerosol (*via* sulphuric acid), which is divided between the Aitken and accumulation modes in proportion to their surface areas.

The scheme is mainly based on the work of *Jenkin* [1996] and *Koga and Tanaka* [1999]. Rate coefficients have been taken from *Atkinson et al.* [1997] where possible. *Koga and Tanaka* [1999] show that their model is capable of reproducing the observed behaviour of the molar ratio of MSA to non-sea-salt sulphate with the assumption of a 10% product yield of MSA from the addition reaction of DMS with OH, and this has been adopted here. The sensitivity of their model to rate coefficients was also examined, where laboratory determinations are not available; two of the rate coefficients used here are taken from the best fit case of the *Koga and Tanaka* model.

The assumption (a) that reactions of DMS with other species are negligible is debatable, since its reaction with NO_3 may be significant at night, when OH is absent. However, *Ravishankara et al.* [1997] argued that the removal of NO_3 due to uptake by sea-salt aerosol may prevent NO_3 playing an important role in the oxidation of DMS in the marine boundary layer. With regard to assumption (b), if any of the intermediate species that occur between DMS and the formation of CH_3SO_2 were to have lifetimes which are comparable in magnitude to that of DMS, the distributions of DMS and its products would be different due to transport processes. Given the complexity of DMS chemistry this possibility cannot be excluded, but the assumption is felt to be reasonable in the context of a climate model.

4.2. SO_2 Oxidation

The conversion of SO_2 to sulphate proceeds *via* two routes: oxidation by OH in the gas phase and by H_2O_2 in solution in cloud droplets. The rate of the gas phase reaction is given by the following expressions, which closely approximates the rate in the STOCHEM model:

$$\frac{d[S_{SO_2}]}{dt} = -k_{lo}(1+k_r)^{-1} \times 0.6^{\alpha}[S_{SO_2}]N_{OH} \tag{13}$$

where

$$\alpha = \frac{1}{1+(0.9693\log_{10} k_r)^2} \tag{14}$$

and

$$k_r = \frac{k_{lo}}{k_{hi}} \ . \tag{15}$$

$[S_{SO_2}]$ is the mass mixing ratio of sulphur as SO_2 and N_{OH} is the number of molecules of OH per cm^3. The reaction rate limits at low and high pressure, k_{lo} and k_{hi} respectively, are given by:

$$k_{lo} = 3 \times 10^{-31} N_{air}(300/T)^{3.3} \tag{16}$$

and

$$k_{hi} = 1.5 \times 10^{-12} \tag{17}$$

where N_{air} is the number of molecules of air per cm^3 and T is the temperature in K. Concentrations of OH are virtually zero at night, so this reaction is then turned off. Accordingly,

the daytime average concentration of OH rather than its diurnal average is used in the rate equation.

The aqueous phase reaction is known to proceed on a timescale shorter than the model's timestep of 30 minutes (see, for example, *Penkett et al.* 1979, *Hegg and Hobbs* 1981 and *Snider and Vali* 1994). It is also a significant sink of H_2O_2. It is therefore parametrized by converting an amount of SO_2 equal (in molar terms) to the lesser of the concentrations of H_2O_2 and SO_2, and depleting an equal molar amount of H_2O_2. This is done only in the cloudy portion of a grid box, and only in the presence of liquid water (it is assumed that no aqueous phase oxidation takes place in ice cloud). If the concentration of H_2O_2 were reset to its prescribed value on the next timestep there would be a serious overestimate of the rate of aqueous phase oxidation, so instead the H_2O_2 is gradually replenished using the prescribed concentration of HO_2, using the reaction rate used in the STOCHEM model:

$$\frac{d[H_2O_2]}{dt} = (2.3 \times 10^{-13} e^{600/T} + 1.9 \times 10^{-33} N_{air}\, e^{890/T}) \times (1 + 1.4 \times 10^{-21} N_{water}\, e^{2200/T})(N_{HO_2})^2. \quad (18)$$

$[H_2O_2]$ is the mass mixing ratio of hydrogen peroxide, N_{water} the number of water vapour molecules per cm^3 and N_{HO_2} the number of HO_2 molecules per cm^3. As with OH, HO_2 concentrations are negligible after dark, so this replenishment reaction is also turned off at night. Note also that $[H_2O_2]$ is never permitted to exceed the mass mixing ratio prescribed from the STOCHEM field. In these experiments, in common with others (*e.g. Chin et al.* 1996, *Kasibhatla et al.* 1997), aqueous phase oxidation by ozone is omitted. The reaction rate of SO_2 with O_3 is highly *p*H dependent, reducing as more sulphate is produced, so that this reaction has a tendency to be self-limiting. *Lohmann and Feichter* [1997] found in their modelling studies that between 3% and 12% of the SO_2 was converted by this mechanism annually, although the proportion increased in boreal winter and decreased in summer. *Barth et al.* [2000] reported various values of this fraction, up to 15.7%.

4.3. Inter-modal Exchanges

Sulphate produced by aqueous phase oxidation is added to the dissolved sulphate variable, whereas sulphate produced by gas phase oxidation is split between the Aitken and accumulation modes in proportion to their surface areas. The following transfers between the three modes of sulphate are parametrized: (i) evaporation of dissolved sulphate to form accumulation mode sulphate in cloud-free areas; (ii) nucleation of cloud droplets on accumulation mode sulphate in cloud to form dissolved sulphate; and (iii) diffusion of interstitial Aitken mode particles into cloud droplets to form dissolved sulphate. The first two of these processes are assumed to occur on a timescale much shorter than the model timestep, so that any dissolved sulphate in the cloud-free part of the grid box is instantaneously converted to the accumulation mode, and all of the accumulation mode entering cloud is instantaneously converted to dissolved sulphate. The diffusion of Aitken mode sulphate into cloud droplets is a much slower process, and is parametrized using the arguments of *Twomey* [1977] to obtain an equation for the diffusive lifetime of Aitken mode particles, τ_{diff} :

$$\tau_{diff} = \rho_w^{\frac{1}{3}} (7.8\, q_c^{\frac{1}{3}}\, \rho_o^{\frac{1}{3}}\, N_d^{\frac{2}{3}}\, \mathrm{D})^{-1} \quad (19)$$

where D is a representative diffusion coefficient for Aitken mode particles, taken as 1.71×10^{-9} $m^2 s^{-1}$.

Coagulation of the free particle modes is not represented in the model at present as it occurs on a longer timescale than the other exchange processes, though it is recognised that the omission of coagulation will tend to increase the ratio of Aitken mode sulphate mass to

accumulation mode mass in the model. As the deposition efficiencies of the two modes of particle differ this implies a change in the overall sulphate burden. It is difficult to quantify the exact size of this since the coagulation process is inherently non-linear, but the neglect of coagulation is not considered to be too serious a drawback.

4.4. Dry Deposition

Dry deposition of all sulphur species except DMS (for which deposition is neglected) is parametrized using an approach analogous to electrical resistances, similar to many previous studies; see, for instance, *Seinfeld and Pandis* [1998]. In the present model, the reference height is effectively at the middle of the layer closest to the surface, and the aerodynamic resistance (r_a) is computed by the stability-dependent boundary-layer mixing scheme. The quasi-laminar resistance (r_b) is computed by first diagnosing the value of r_b for water vapour implied by the boundary-layer/surface scheme, and then scaling this using the relation $r_b \propto \mathrm{D}^{-2/3}$, as suggested by *Monteith and Unsworth* [1990]; D is the molecular diffusivity in the case of water vapour and SO_2, or an appropriate particle diffusivity for the free particle modes. The resistance to uptake at the surface (r_c) is set to zero for particles, *i.e.* bouncing off and resuspension are neglected. For SO_2, r_c is set to zero over ocean; over land it is computed from the stomatal resistance used for water vapour, using the scaling relation $r_c \propto \mathrm{D}^{-1}$. The turbulent deposition of sulphate dissolved in cloud droplets (sometimes known as 'occult' deposition) is assumed to be relatively efficient due to the processes of sedimentation and impaction, as discussed by *Monteith and Unsworth* [1990], so both r_b and r_c are set to zero for this mode.

4.5. Wet Deposition

The HadAM4 model treats large-scale cloud and convective cloud separately and quite differently, and so the parametrization of wet deposition also differs in the two cases. Consider first the treatment of deposition by large-scale precipitation. The scavenging of SO_2 by snow is neglected; for scavenging by rain, the removal rate is parametrized by:

$$\frac{\partial S}{\partial t} = -\Lambda(\Psi, S)\, S \tag{20}$$

where S stands for the volumetric concentration of SO_2 in parts per billion, Ψ is the grid-box mean precipitation rate in units of mm hr^{-1}, and the scavenging coefficient Λ is given by

$$\Lambda(\Psi, S) = \begin{cases} \lambda_0 \Psi^{2/3} & \text{if } S \le S_0, \\ \lambda_1 (\Psi/S)^{2/3} & \text{if } S > S_0. \end{cases} \tag{21}$$

The constants in this equation are assigned the values $\lambda_0 = 6.5 \times 10^{-5}\mathrm{s}^{-1}$, $\lambda_1 = 2.955 \times 10^{-5}\mathrm{s}^{-1}$, and $S_0 = 0.3065$ ppbv, so that Λ is a continuous function of S. Note that the parametrization has the property that, in polluted air, the scavenging coefficient falls as S increases (at fixed Ψ), due to raindrops becoming saturated with SO_2.

Rainout of sulphate dissolved in cloud droplets is modelled by assuming that the concentration of dissolved sulphate is uniform within the clouds in a grid box, so that if a certain proportion of the condensed water is removed as precipitation, the same proportion of dissolved sulphate is also removed. If the precipitation completely evaporates at a level, any removal above that level is suppressed. However, the effect of partial evaporation of precipitation below cloud base is not treated; this will clearly tend to overestimate wet deposition. Conversely, scavenging of sulphate particles by falling precipitation ('washout') is not represented, partly to compensate for the aforementioned overestimation and also because it is generally believed to be less important than rainout. (This approximation has

been made in some previous studies, for example those of *Langner and Rodhe* 1991 and *Kasibhatla et al.* 1997).

Turning next to scavenging by convective precipitation, there is no explicit link with the dissolved sulphate variable as this is associated only with stratiform cloud. 'Rainout' is therefore not parametrized in the same way; instead all three modes of particulate sulphate are removed using the (linear) scheme:

$$\frac{\partial[S_{SO4}]}{\partial t} = -\lambda_C \Psi [S_{SO4}], \tag{22}$$

where Ψ is here the total precipitation rate, including snow, $\lambda_C = 3 \times 10^{-5} \mathrm{s}^{-1}$, and the important assumption is made that for this purpose the convective precipitation takes place over just 5% of the horizontal area of the grid box. This area assumption is also made when scavenging SO_2, but in that case the nonlinear scheme described above for large-scale precipitation is used. Finally, wet deposition of DMS is not represented at all.

4.6. Emissions

Three sources of atmospheric sulphur are represented in the model. Anthropogenic emissions of SO_2 are taken from the 1B inventory compiled under the auspices of GEIA, the Global Emissions Inventory Activity of IGAC, the International Global Atmospheric Chemistry project (information on GEIA can be found at http://www.geiacenter.org). This inventory represents the situation in the mid-1980s, since when emissions have been reduced in many developed countries, such as the United States and most Western European states, but may have increased in some developing nations. Thus the results of the experiments to be described below are not, strictly speaking, representative of present-day conditions. The inventory divides the emissions into those taking place at or very near the surface, and those from elevated sources such as power station chimney stacks. This division is reflected in the model by injecting the elevated emissions directly into the seventh model layer above the surface (see Appendix A), while the near-surface emissions are introduced as specified surface fluxes in the boundary layer mixing scheme. The global total of the anthropogenic emissions is 67 Tg(S) per annum.

Volcanic emissions are taken from the dataset of *Andres and Kasgnoc* [1998], also available from GEIA. This inventory is split into contributions from more-or-less continually erupting volcanoes on the one hand and sporadic eruptions on the other. It is not obvious how to handle the effects of the sporadic eruptions in a modelling study that attempts to simulate average conditions. The approach adopted here is to neglect the sporadic volcanoes entirely; thus the estimated indirect anthropogenic forcing will be representative of years when no major (sporadic) eruption occurs. *Andres and Kasgnoc* estimated that 64% of the global volcanic emissions of sulphur occur in the form of SO_2, with the remainder appearing in a variety of compounds as well as particulate sulphur. For simplicity, these remaining emissions are assumed to occur as SO_2 in the present experiments. The volcanic emissions are injected at a constant rate into layers 9 to 22 of the model, with the mass distributed uniformly through the layers. The global total of the volcanic emissions is 7.5 Tg(S) per annum.

The other natural source of atmospheric sulphur represented in the model is DMS of biological origin, mainly from the ocean where it is (indirectly) produced by certain species of plankton, as discussed by *Liss et al.* [1997]. There is considerable uncertainty regarding the size and distribution of the flux of DMS from the ocean to the atmosphere. This study uses the estimates compiled by *Kettle et al.* [1999], based on measurements of DMS concentrations in seawater made by many workers, combined with climatological surface wind speeds and the *Liss and Merlivat* [1986] parametrization of air-sea gas exchange. The seasonal variation in DMS emissions is very important, so the model interpolates in time

between fields of monthly mean estimated fluxes. The global marine DMS emission is equivalent to 19.2 Tg(S) per annum. In addition there is a relatively small contribution from the continents, where vegetation and soils emit both DMS and H_2S. For simplicity, these biogenic emissions from land are treated as if they were entirely of DMS. The emissions estimates used are from *Spiro et al.* [1992]: the global continental DMS emission is equivalent to 0.9 Tg(S) per annum.

5. Experimental Design

Estimates of the radiative effects of aerosols are usually quoted in terms of *radiative forcing*. This term can be defined as the radiative impact of an instantaneous change in some component of the climate system (*e.g.* sulphate aerosol concentration), without any subsequent effects of this change being allowed to feed back on the system. However, this approach cannot be taken with the second indirect effect: aerosol-induced changes in N_d must be allowed to feed back to allow the effect to develop. Consequently, to determine the radiative impact of sulphate changes due to this mechanism, a different approach must be taken. Pairs of climate model integrations are run in parallel, one using 'pre-industrial' (natural only) sulphur emissions, the other using 'modern' (natural plus anthropogenic) emissions, and the difference in net cloud radiative forcing between the two runs provides an estimate of the aerosol's radiative impact. As changes due to the indirect effects are allowed to feed back on the system, this radiative impact is not, technically speaking, a forcing, although the term will occasionally be used in a loose sense. Note that the direct effect of the modelled sulphate aerosol is omitted from all runs. The simulations are run for five years (after an initial 3-month spin-up period) to allow the random changes between the simulations to average out and so let the aerosol-induced signal be seen more clearly.

Six experiments were conducted, each consisting of two parallel five year runs of the GCM, as follows:

1. BOTH: first (albedo) and second (lifetime) indirect effects combined;
2. FIRST: first indirect effect only;
3. SECOND: second indirect effect only;
4. BOTH-acv: both effects, alternative parametrization of autoconversion;
5. BOTH-DMS: both effects, alternative DMS emissions;
6. BOTH-fix: both effects, non-interactive seasonal-mean aerosols.

Experiments BOTH, FIRST and SECOND were conducted to obtain an estimate of the combined indirect effect *via* both mechanisms, and to obtain estimates of the relative magnitude of the two effects. In FIRST, the lifetime effect was deactivated by providing the precipitation scheme in both the pre-industrial and modern-day runs with non-interactive, seasonally-varying aerosol concentration fields obtained from the 'pre-industrial' run of BOTH. The same fields were used in the radiation scheme to deactivate the albedo effect in SECOND.

Experiment BOTH-acv explored the uncertainty in the parametrization of the autoconversion process: the parametrization of *Beheng* [1994] was substituted for the standard *Tripoli and Cotton* scheme (Eq. 5). BOTH-DMS was performed to investigate the sensitivity of the indirect effects to uncertainties in natural aerosol concentrations: in the standard case (BOTH), DMS emissions are specified based on the parametrization of *Liss and Merlivat* [1986] for air-sea gas exchange, whereas in BOTH-DMS an alternative parametrization (*Wanninkhof* 1992) is used. Finally, to assess the importance of using interactive aerosols compared with using prescribed aerosol distributions (as used by *Jones and Slingo* 1996 and *Rotstayn* 1999), seasonal-mean distributions of pre-industrial and modern-day aerosol were created from BOTH and used as non-interactive input to BOTH-fix.

6. Results

The modern and pre-industrial distributions of annual mean total column sulphate from BOTH are shown in Fig. 1(a & b). The spatial pattern of the modern distribution (Fig. 1a) is fairly similar to that simulated in previous modelling studies (for instance *Langner and Rodhe* 1991), with maxima near and downwind of the major industrial source regions. There is a pronounced seasonal cycle, with much higher concentrations of sulphate in summer than in winter. This is mainly due to higher oxidant concentrations in summer (the result of larger fluxes of photolytically-active shortwave radiation), reinforced by the effect of seasonal changes in precipitation. In the map of the pre-industrial sulphate burden (Fig. 1b), the most prominent maxima are due to volcanic emissions. Because these are injected well above the surface they are less readily deposited than the near-surface emissions of anthropogenic sulphur and therefore make a relatively larger contribution to the sulphate loading than might be expected from the total volcanic emission figure, as noted by *Chin and Jacob* [1996].

Annual mean concentrations of the dry sulphate mass (*i.e.* the sum of the Aitken and accumulation modes) in the lowest layer of the model from the modern-day run of BOTH are compared with measurements near the surface in Fig. 2(a & b). Sulphate dissolved in cloud droplets is excluded from the model values for the purposes of this comparison, under the assumption that this would not be sampled by the instruments used to make the measurements. The value at the closest model grid point to the measurement site has been taken. Fig. 2(a) contains selected stations from the EMEP (Co-operative Programme for Monitoring and Evaluation of the Long Range Transmission of Air Pollutants in Europe) network in Europe; it should be noted that the observations are of total sulphate, *i.e.* the sea-salt sulphate contribution has not been subtracted. On the other hand, in Fig. 2(b), which contains selected stations from the University of Miami database (*Savoie and Prospero*, personal communication, 1999), the values are of non-sea-salt sulphate. The stations selected from this database are remote from sources of pollution and are from various coastal and oceanic sites around the globe. The EMEP data have in each case been averaged over the 4 years 1986-89 inclusive. Data for subsequent years are available, but have been excluded from the comparison because of the significant changes in European emissions that have taken place since 1990: recall that the anthropogenic emissions inventory represents the position in the mid-1980s. Stations in the University of Miami database that may be affected by local sources, or that were not operational during at least some part of the 1980s, have been excluded. The results indicate that the model predictions of sulphate concentrations in regions generally remote from pollution sources (Fig. 2b) compare fairly well with the observations, but in more polluted regions (Fig. 2a) the model underpredicts to a degree.

The global annual mean aerosol burdens in BOTH are equivalent to approximately 0.25 Tg(S) in the pre-industrial case and 0.66 Tg(S) in the modern case. These are within the range covered by previous modelling studies: estimates of the modern sulphate burden in Tg(S) have included 1.05 (*Lelieveld et al.* 1997), 0.96 (*Roelofs et al.* 1998), 0.80 (*Pham et al.* 1995), 0.63 (*Feichter et al.* 1996), 0.60 (*Rasch et al.* 2000), 0.55 (*Chuang et al.* 1997a) and 0.53 (*Chin and Jacob* 1996). While there is some variation in the emissions datasets used in these studies, much of the range in aerosol loading is likely to be due to differences in the formulation of the models. The tendency to underpredict the sulphate concentrations over Europe in the present model may be associated with the absence of aqueous phase oxidation of SO_2 by ozone, in view of the results of *Rasch et al.* [2000], who found that this reaction was unusually significant over Europe.

The model's simulation of cloud droplet effective radius was assessed by comparison with the satellite retrievals of *Han et al.* [1994] and *Kawamoto* [1999], the modelled distribution of r_e being taken from the modern-day run of BOTH. Composite distributions of the r_e retrievals were produced by taking the mean of the retrievals from January, April, July and October 1987. These were compared with a similar composite from the model

using the 5-year mean r_e values from the same 4 months. As the same missing-data mask was applied to all three distributions, this limits the comparison to approximately 50°N to 40°S, the latitudinal range of the *Han et al.* retrievals. Table 2 shows that the modelled r_e is within the 1–2μm uncertainty quoted for the *Han et al.* retrievals, and that in general there is as much discrepancy between the different retrievals as there is between the model and the retrievals. Over land (Fig. 3a) the retrievals are generally offset from each other by 1–2μm, agreeing more closely as one approaches the latitudinal limits of the retrievals. The modelled r_e values are in broad agreement with both, the largest difference being the lack in the model of the sharp dip in r_e at around 20°N associated with retrievals over the Sahara. Over the oceans (Fig. 3b), the retrievals agree fairly closely with each other and with the model in the tropics, but then all three diverge towards higher latitudes.

The impact of anthropogenic sulphate aerosols on shortwave, longwave and net cloud forcing in the six experiments, averaged over the five years of the runs, is given in Table 3 (values are presented as 'modern' minus 'pre-industrial'). Also given are the associated changes in global annual-mean cloud liquid water path (LWP) and the absolute change in percentage cloud cover. The ranges of net cloud forcing quoted are the standard deviations obtained by treating the individual annual means of the 5-year simulations as independent samples. These results indicate that the shortwave 'cooling' effect due to brighter clouds is generally an order of magnitude greater than the longwave 'warming' effect due to higher LWPs. This is because the longwave cloud forcing associated with the types of low-level liquid water clouds under consideration here is weak compared with their shortwave forcing.

The distributions of the indirect radiative impacts from BOTH, FIRST and SECOND are shown in Fig. 4(a–c) respectively. There are forcing peaks adjacent to the main sources of sulphur emissions in the north-eastern USA, Europe and China, and also over the main regions of marine stratocumulus off the western coasts of Africa and America. The global mean for the total indirect effect (Fig. 4a) of -1.89 Wm^{-2} is similar to the value of -2.1 Wm^{-2} obtained by *Rotstayn* [1999]. *Lohmann et al.* [2000] obtained a value of -1.9 Wm^{-2} in one of their experiments ('PROG-N_d-min') where they reduced their global-mean value of minimum cloud droplet concentration (N_{min}) from their standard value of 40 cm^{-3} to 10 cm^{-3}, a value much closer to the global-mean N_{min} value of 12.8 cm^{-3} used in this study (the mean of the 5 cm^{-3} over ocean and land-ice sheets and the 35 cm^{-3} elsewhere over land). However, it should be noted that *Lohmann et al.* were considering anthropogenic changes in aerosols other than just sulphate.

A comparison of FIRST and SECOND with BOTH shows that the forcings due to the first and second indirect effects add more or less linearly in the combined effect, with the first effect dominating in a ratio of approximately 3:1. This partitioning of the two effects is broadly consistent with the findings of *Lohmann and Feichter* [1997] and *Rotstayn* [1999], but is the reverse of the results of *Lohmann et al.* [2000].

Although the forcing of -1.89 Wm^{-2} in BOTH is similar to the range of forcings quoted by *Lohmann and Feichter* [1997] and *Lohmann et al.* [2000], the latter were obtained using a different autoconversion scheme to that used in HadAM4. To examine the sensitivity of estimates of the indirect effect to the parametrization of this process, BOTH-acv used the scheme of *Beheng* [1994] instead of the standard one based on *Tripoli and Cotton* described above. As used by *Lohmann and Feichter* [1997] and *Lohmann et al.* [2000] in the ECHAM4 model, this alternative parametrization gives R_{auto} as:

$$R_{auto} = \frac{6 \times 10^{28}\, \gamma_1\, (\rho_o\, q_c \times 10^{-3})^{4.7}}{n^{1.7} (N_d \times 10^{-6})^{3.3} \rho_o} \tag{23}$$

where γ_1 is a tunable efficiency parameter (=220) and n is a parameter related to the droplet spectrum width (=10); the other quantities are as before. Clearly the *Beheng* scheme has a stronger dependence on cloud water content and droplet concentration compared with the standard scheme, and so not surprisingly the use of this parametrization leads to a considerable increase in the combined indirect effect by a factor of about 2 to -3.68 Wm^{-2}.

The much larger changes in LWP associated with the *Beheng* parametrization are evident in the values shown in Table 3: whilst all other experiments which include the second indirect effect show an increase in LWP of the order of 5% compared with each experiment's pre-industrial run, the increase in BOTH-acv is more than 20%. This is broadly consistent with the 17.1% LWP increase obtained by *Lohmann and Feichter*. *Rotstayn* [1999] obtained an increase in LWP of a similar order of magnitude (6%) to those shown in Table 3 (excepting FIRST and BOTH-acv) using a version of the CSIRO model, which is consistent with the use of the *Tripoli and Cotton* autoconversion rate in that model.

Another area of uncertainty concerns natural aerosol concentrations. These are important as they control the susceptibility of clouds to anthropogenic change. Pre-industrial sulphate aerosol concentrations are strongly affected by the emission of DMS from the oceans. In BOTH, DMS emission fluxes were based on the air-sea gas exchange parametrization of *Liss and Merlivat* [1986], whereas in BOTH-DMS they were based on an alternative parametrization, that of *Wanninkhof* [1992]; both schemes parametrize air-sea exchange in terms of windspeed. The study of *Nightingale et al.* [2000] compares these schemes with field measurements, finding that the observations tend to scatter between the two parametrizations, and they suggest that factors other than windspeed may be important in controlling the exchange. The DMS emissions in BOTH-DMS are roughly twice those in BOTH, and the effect this has on increasing the natural (or 'background') aerosol distribution, thereby decreasing the susceptibility of clouds to anthropogenic influence, is clear in the reduction of the total indirect effect by over 25% to -1.38 Wm^{-2}. This result demonstrates the importance of the natural background cloud droplet distribution in attempting to estimate indirect forcing.

Comparing the radiative impacts from BOTH and BOTH-fix indicates the impact of using prescribed sulphate distributions. By design these experiments have the same annual-mean sulphate burdens, yet the radiative impact determined using non-interactive seasonal-mean prescribed aerosol fields (BOTH-fix) overestimates the total indirect effect by approximately 17%. This suggests a preference for the interactive modelling of aerosols within GCMs. This result is similar to that noted previously by *Feichter et al.* [1997]. They found an increase of 20% in indirect forcing when using time-mean sulphate fields, but the results are not strictly comparable: *Feichter et al.* considered only the first indirect effect and used monthly-mean sulphate data, whereas here we consider both indirect effects and use seasonal-mean aerosol fields.

7. Discussion and Conclusions

A series of experiments has been conducted to make estimates of the total indirect effect of anthropogenic sulphate aerosols, both *via* increases in cloud albedo and *via* changes to the precipitation efficiency of clouds. The experiments used a version of the HadAM4 GCM with an interactive sulphur cycle, a diagnostic treatment of sea-salt aerosol and a new cloud microphysics scheme. The main conclusions from the experiments are:

1. that the total indirect radiative impact of anthropogenic sulphate aerosols is approximately -1.9 Wm^{-2};
2. that this value is uncertain to within at least a factor of 2;
3. that the second indirect effect is of a comparable order of magnitude to the first;
4. that the shortwave (cooling) impact of the second effect dominates its longwave (warming) impact;
5. that estimating indirect forcing using non-interactive aerosol fields can introduce a significant error.

The uncertainty in the value of the total indirect effect is associated both with the 'inputs' (*i.e.* the specification of the aerosol distribution) and with the 'processes' (*i.e.* the

parametrization schemes). The sulphate and sea-salt aerosols which are modelled in this study (one prognostically and one diagnostically) are only two components of the atmospheric aerosol which is usually much more complex in composition. Other species which may be of importance include carbonaceous aerosols (both black and organic), nitrates and mineral dust, many of which occur as components of CCN. The impact of these non-sulphate aerosols depends on the relative degree to which they affect the pre-industrial and the modern-day concentration of cloud droplets, *i.e.* to what degree they are natural or anthropogenic. Even considering sulphate alone there is considerable uncertainty: for example, different methods of parametrizing the sea-air flux of DMS lead to a difference of about 25% in the estimated forcing. Related to the question of aerosol composition is that of the relationship between aerosol and cloud droplet number concentrations. Improvements to the relations currently used will require a greater understanding of the complex processes involved in cloud nucleation (*e.g. Chuang et al.* 1997b, *Hallberg et al.* 1998) as well as improvements in the modelling of the CCN distributions used as input. The study of *Lohmann et al.* [2000], for example, is an interesting development in this direction, although a large range of uncertainty still results.

A further source of uncertainty is illustrated by the experiments which use different parametrizations of the autoconversion rate. These demonstrate a significant sensitivity to this process, with the capacity to double the estimate of the total indirect effect, even though the lifetime effect only contributes some 25% of the total effect in the standard case. Although it would seem that a negative forcing of the magnitude obtained in BOTH-acv must be incorrect (by arguing that such a negative forcing would have overwhelmed the warming due to greenhouse gases, and thus produced global cooling over the past 250 years, not the warming observed), there is always the possibility that this forcing is largely offset by some hitherto unidentified positive forcing. Even if no such positive forcing exists, one still cannot use the magnitude of the indirect forcing produced by the *Beheng* scheme as evidence against the parametrization: the values of droplet concentration used as input could be at fault. The range of possible results that the uncertainty in this process implies clearly requires further study of this complex and highly non-linear process. The fact that we find similar degrees of uncertainty associated with both 'inputs' and 'processes' differs from the conclusion of *Pan et al.* [1998] who found a far larger uncertainty connected with the inputs ('parametric uncertainty') compared with the processes ('structural uncertainty'). However, their study was concerned only with the first indirect effect, whereas the large 'structural uncertainties' we find are associated with the parametrization of the autoconversion process central to the second indirect effect.

Most of the early attempts to estimate the (first) indirect effect used non-interactive aerosol fields — for example, *Jones et al.* [1994] used annual-mean sulphate data. Conclusion 5 suggests that if climate or numerical weather prediction models are to include schemes in which cloud properties are allowed to depend on aerosol distributions, the use of prescribed aerosol climatologies may give unsatisfactory results even if the climatologies themselves are reliable. The fundamental reason for this is that the relation between the aerosol and cloud droplet concentrations is nonlinear, so that using input aerosol concentrations meaned over any period longer than the timescale on which aerosols evolve will introduce an error. Appendix B discusses this question in more depth, and contains an argument explaining how the exact form of the parametrization linking the aerosol and cloud droplet concentrations (Eq. 4) leads to magnified estimates of the size of the indirect effect in the experiment with prescribed sulphate distributions (BOTH-fix). The opposite possibility, that alternative parametrizations might, when driven by non-interactive aerosol fields, yield estimates of the size of indirect forcing that are too small, cannot be excluded. However, since any physically reasonable parametrization will be nonlinear, the use of non-interactive aerosol fields is highly likely to introduce significant error (barring a fortuitous cancellation of the errors in the pre-industrial and anthropogenically-perturbed cases).

Nevertheless, despite these uncertainties, these results suggest that the indirect effects

of aerosols on clouds are important and that they need to be taken into account when considering human influence on climate: the estimate of -1.89 Wm^{-2} for the total indirect effect would offset a large fraction of the forcing caused by the increases in greenhouse gases to date.

Appendix A

Vertical co-ordinates of HadAM4

The GCM uses a hybrid vertical co-ordinate system which varies smoothly from a pure sigma co-ordinate (pressure divided by surface pressure) near the surface to a pure pressure system towards the top of the model. Pressure (p) at a given level is given by $p = \mathrm{A} + \mathrm{B}p^*$, where p^* is the surface pressure (Pa). The values of the coefficients A and B for the boundaries of the model layers are given below with boundary 0 indicating the surface:

Boundary	A	B
38	50.0	0.0
37	1000.0	0.0
36	2000.0	0.0
35	4000.0	0.0
34	6333.6	0.001664
33	8345.4	0.006546
32	10051.6	0.014484
31	11468.6	0.025315
30	12612.6	0.038874
29	13500.2	0.054998
28	14147.4	0.073526
27	14570.8	0.094292
26	14786.6	0.117134
25	14811.1	0.141889
24	14660.6	0.168394
23	14351.6	0.196484
22	13794.3	0.232057
21	12781.4	0.282186
20	11521.2	0.334788
19	9700.1	0.402999
18	7825.4	0.479726
17	5345.5	0.556545
16	3500.4	0.624996
15	2064.1	0.684359
14	1045.7	0.734543
13	409.0	0.775910
12	87.8	0.809122
11	0.0	0.835000
10	0.0	0.858000
9	0.0	0.8800
8	0.0	0.9010
7	0.0	0.9210
6	0.0	0.9400
5	0.0	0.9580
4	0.0	0.9719
3	0.0	0.9835
2	0.0	0.9929
1	0.0	0.9976
0	0.0	1.0

Appendix B

The aim of this appendix is to shed some light on the question of why using prescribed time-average aerosol fields produces estimates of indirect effects that are in general different from, and in the particular case of the present study stronger than, those obtained with interactive aerosol fields. The arguments to be presented are not a proof, but they do provide useful insight into the behaviour of the model.

The discussion revolves around the form of the function linking cloud droplet number concentration N_d with the aerosol number concentration A. Reduced to its mathematical essentials, this is:

$$N_d(A) = \begin{cases} N_\infty(1 - e^{-\lambda A}) & \text{if } A > A_m, \\ N_m & \text{if } 0 \leq A \leq A_m. \end{cases} \tag{B1}$$

Here N_m is the minimum value of N_d at low aerosol concentrations, N_∞ is the asymptotic limit of N_d as $A \to \infty$, λ is a constant and A_m is such that $N_m = N_\infty(1 - e^{-\lambda A_m})$.

For $A > A_m$,

$$N_d''(A) = -\lambda^2 N_\infty e^{-\lambda A} < 0, \tag{B2}$$

so that the function is concave (for $A > A_m$). Now for a concave function $f(x)$, with x taking on a distribution of values either in space, time or as a random variable, and with an overbar denoting an average or probabilistic expectation, Jensen's inequality states that:

$$f(\overline{x}) \geq \overline{f(x)}, \tag{B3}$$

i.e. using the mean value of x as input to f produces an output that overestimates the true mean of f. (Actually, Jensen's inequality is normally proved for convex functions, in which case the direction of the inequality is reversed; see *e.g. Feller* 1966.)

Thus in the anthropogenically-perturbed situation where $A \gg A_m$ most of the time, it is to be expected that $N_d(\overline{A}) > \overline{N_d(A)}$, *i.e.* using the mean aerosol concentration will overestimate the true average droplet concentration.

In contrast, if $A < A_m$ then $N_d(A)$ is not concave. Indeed, if $\overline{A} \leq A_m$ then $N_d(\overline{A}) = N_m \leq \overline{N_d(A)}$, *i.e.* using the mean aerosol concentration will underestimate the true average droplet concentration. This situation is likely to occur quite frequently in the pre-industrial experiments. The result of a tendency to underestimate N_d in the pre-industrial case and overestimate it in the modern case would be that the size of the indirect effect would be exaggerated.

If $\overline{A} > A_m$ but the distribution of A does extend significantly below A_m, then it seems that no general statement about the relative sizes of $N_d(\overline{A})$ and $\overline{N_d(A)}$ can be made (without making further assumptions about the distribution of A). Therefore it is difficult to prove that using average aerosol fields must exaggerate the strength of indirect forcing. However, the above arguments make it very plausible that this is likely to occur when N_d is parametrized in the way chosen here.

Although there is much uncertainty about the best way to parametrize the relation between A and N_d, one would expect the concavity property to be realistic: as A increases, the competition between the different aerosol particles for the available water vapour will result in N_d rising more and more slowly. Note that the key element in making the error in the indirect effect an *over*estimate when using average aerosols is the use of a minimum cloud droplet number concentration N_m. If $N_d(A)$ were concave everywhere, then the cloud droplet number concentration would be overestimated in both the anthropogenically-perturbed and pre-industrial experiments (with mean aerosol). In that case the error due to using specified time-average fields could take either sign; one would nevertheless anticipate a significant error unless the averaging period were so small as to be comparable with the timescale on which aerosol fields evolve. Any averaging period greater than a day is unlikely to be adequate.

Acknowledgements We wish to thank Kazuaki Kawamoto (NASA Langley) for making his satellite retrievals available to us. We are grateful to D. L. Savoie and J. M. Prospero (Rosenstiel School of Marine and Atmospheric Science, University of Miami) for permission to cite data from their aerosol database; we are equally grateful to those involved in assembling the EMEP dataset. This work was supported by the UK Department of the Environment, Transport and the Regions under contract PECD 7/12/37.

References

Ackerman, A. S., O. B. Toon and P. V. Hobbs, Numerical modelling of ship tracks produced by injection of cloud condensation nuclei into marine stratiform clouds, *J. Geophys. Res., 100*, 7121-7133, 1995.

Albrecht, B. A., Aerosols, cloud microphysics and fractional cloudiness, *Science, 245*, 1227-1230, 1989.

Andres, R. J. and A. D. Kasgnoc, A time-averaged inventory of subaerial volcanic sulfur emissions, *J. Geophys. Res., 103*, 25251-25261, 1998.

Atkinson, R., D. L. Baulch, R. A. Cox, R. F. Hampson, J. A. Kerr, M. J. Rossi and J. Troe, Evaluated kinetic, photochemical, and heterogeneous data for atmospheric chemistry: Supplement V, *J. Phys. Ref. Data, 26*, 1997.

Ayers, G. P., J. M. Cainey, H. Granek and C. Leck, Dimethylsulfide oxidation and the ratio of methanesulfonate to non sea-salt sulfate in marine air, *J. Atmos. Chem., 25*, 307-325, 1996.

Barth, M. C., P. J. Rasch, J. T. Kiehl, C. M. Benkovitz and S. E. Schwartz, Sulfur chemistry in the National Center for Atmospheric Research Community Climate Model: Description, evaluation, features, and sensitivity to aqueous chemistry, *J. Geophys. Res., 105*, 1387-1415, 2000.

Beheng, K. D., A parameterization of warm cloud microphysical conversion processes, *Atmos. Res., 33*, 193-206, 1994.

Boucher, O. and U. Lohmann, The sulfate-CCN-cloud albedo effect: A sensitivity study with two general circulation models, *Tellus B, 47*, 281-300, 1995

Bower, K. N., T. W. Choularton, J. Latham, J. Nelson, M. B. Baker and J. Jensen, A parametrization of warm clouds for use in atmospheric general circulation models, *J. Atmos. Sci., 51*, 2722-2732, 1994.

Chin, M. and D. J. Jacob, Anthropogenic and natural contributions to tropospheric sulfate: a global model analysis, *J. Geophys. Res., 101*, 18691-18699, 1996.

Chin, M., D. J. Jacob, G. M. Gardner, M. S. Foreman-Fowler, P. A. Spiro and D. L. Savoie, A global three-dimensional model of tropospheric sulfate, *J. Geophys. Res., 101*, 18667-18690, 1996.

Chuang, C. C., J. E. Penner, K. E. Taylor, A. S. Grossman and J. J. Walton, An assessment of the radiative effects of anthropogenic sulfate, *J. Geophys. Res., 102*, 3761-3778, 1997a.

Chuang, P. Y., R. J. Charlson and J. H. Seinfeld, Kinetic limitations on droplet formation in clouds, *Nature, 390*, 594-596, 1997b.

Collins, W. J., D. S. Stevenson, C. E. Johnson and R. G. Derwent, Tropospheric ozone in a global-scale three-dimensional Lagrangian model and its response to NO_x emission controls, *J. Atmos. Chem., 26*, 223-274, 1997.

Cullen, M. J. P., The unified forecast/climate model, *Meteorol. Mag., 122*, 81-94, 1993.

Cusack, S., J. M. Edwards and R. Kershaw, Estimating the subgrid variance of saturation and its parametrization for use in a GCM cloud scheme, *Q. J. Roy. Meteorol. Soc., 125*, 3057-3076, 1999.

Durkee, P. A., K. J. Noone, R. J. Ferek, D. W. Johnson, J. P. Taylor, T. J. Garrett, P. V. Hobbs, J. G. Hudson, C. S. Bretherton, G. Innis, G. M. Frick, W. A. Hoppel, C. D. O'Dowd, L. M. Russell, R. Gasparovic, K. E. Nielson, S. A. Tessmer, E. Öström, S. R. Osborne, R. C. Flagan, J. H. Seinfeld and H. Rand, The impact of ship-produced aerosols on the microstructure and albedo of warm stratocumulus clouds: A test of MAST hypotheses 1i and 1ii, *J. Atmos. Sci., 57*, 2554-2569, 2000.

Feichter, J., E. Kjellström, H. Rodhe, F. Dentener, J. Lelieveld and G.-J. Roelofs, Simulation of the tropospheric sulfur cycle in a global climate model, *Atmos. Environ., 30*, 1693-1707, 1996.

Feichter, J., U. Lohmann and I. Schult, The atmospheric sulfur cycle in ECHAM-4 and its impact on the shortwave radiation, *Clim. Dyn., 13*, 235-246, 1997.

Feller, W., *An Introduction to Probability Theory and Its Applications, volume II*, John Wiley & Sons, New York, 1966.

Ferek, R. J., T. Garrett, P. V. Hobbs, S. Strader, D. Johnson, J. P. Taylor, K. Nielson, A. S. Ackerman, Y. Kogan, Q. Liu, B. A. Albrecht and D. Babb, Drizzle suppression in shiptracks, *J. Atmos. Sci., 57*, 2707-2728, 2000.

Fowler, L. D. and D. A. Randall, Liquid and ice cloud microphysics in the CSU general circulation model. Part III: Sensitivity to modeling assumptions, *J. Clim., 9*, 561-586, 1996.

Gregory, J. M., Representation of the radiative effect of convective anvils, *Hadley Centre Tech. Note No. 7*, Meteorological Office, Bracknell, UK, 1999.

Hallberg, A., K. J. Noone and J. A. Ogren, Aerosol particles and clouds: which particles form cloud droplets? *Tellus B, 50*, 59-75, 1998.

Han, Q., W. B. Rossow and A. A. Lacis, Near-global survey of effective droplet radii in liquid water clouds using ISCCP data, *J. Clim., 7*, 475-497, 1994.

Hegg, D. A. and P. V. Hobbs, Cloud water chemistry and the production of sulfates in clouds, *Atmos. Environ., 15*, 1597-1604, 1981.

Hegg, D. A., J. Livingston, P. V. Hobbs, T. Novakov and P. Russell, Chemical apportionment of aerosol column optical depth off the mid-Atlantic coast of the United States, *J. Geophys. Res., 102*, 25293-25303, 1997.

Hoppel, W. A., J. W. Fitzgerald, G. M. Frick, R. E. Larson and E. J. Mack, Aerosol size distributions and optical properties found in the marine boundary layer over the Atlantic Ocean, *J. Geophys. Res., 95*, 3659-3686, 1990.

Hudson, J. G. and H. Li, Microphysical contrasts in Atlantic stratus, *J. Atmos. Sci., 52*, 3031-3040, 1995.

IPCC, *Climate Change 1995: The science of climate change*, (eds. J. T. Houghton, L. G. Meira Filho, J. Bruce, H. Lee, B. A. Callander, E. Haites, N. Harris and K. Maskell), Cambridge University Press, 1996.

Jenkin, M. E., Chemical mechanisms forming condensable material, *AEA Technology Report AEA/RAMP/20010010*, AEA Technology, UK, 1996.

Jones, A., D. L. Roberts and A. Slingo, A climate model study of indirect radiative forcing by anthropogenic sulphate aerosols, *Nature, 370*, 450-453, 1994.

Jones, A. and A. Slingo, Predicting cloud droplet effective radius and indirect sulphate aerosol forcing using a general circulation model, *Q. J. R. Meteorol. Soc., 122*, 1573-1595, 1996.

Kasibhatla, P., W. L. Chameides and J. St. John, A three-dimensional global model investigation of seasonal variations in the atmospheric burden of anthropogenic sulfate aerosols, *J. Geophys. Res., 102*, 3737-3759, 1997.

Kawamoto, K., On the global distribution of the water cloud microphysics derived from AVHRR remote sensing. *Center for Climate System Research Report No. 11*, University of Tokyo, Japan, 1999.

Kettle, A. J., M. O. Andreae, D. Amouroux, T. W. Andreae, T. S. Bates, H. Berresheim, H. Bingemer, R. Boniforti, G. Helas, C. Leck, M. Maspero, P. Matrai, A. R. McTaggart, N. Mihalopoulos, B. C. Nguyen, A. Novo, J. P. Putaud, S. Rapsomanikas, G. Roberts, G. Schebeske, S. Sharma, R. Simo, R. Staubes, S. Turner and G. Uher, A global database of sea surface dimethylsulfide (DMS) measurements and a procedure to predict sea surface DMS as a function of latitude, longitude and month, *Global Biogeochemical Cycles, 13*, 399-444, 1999.

Koga, S. and H. Tanaka, Modelling the methanesulfonate to non-sea-salt sulfate molar ratio and dimethylsulfide oxidation in the atmosphere, *J. Geophys. Res., 104*, 13735-13747, 1999.

Kristjánsson, J. E., J. M. Edwards and D. L. Mitchell, A new parametrization scheme for the optical properties of ice crystals for use in general circulation models of the atmosphere, *Phys. and Chem. of the Earth, 24*, 231-236, 1999.

Langner, J. and H. Rodhe, A global three-dimensional model of the tropospheric sulfur cycle, *J. Atmos. Chem., 13*, 225-263, 1991.

Lelieveld, J., G.-J. Roelofs, L. Ganzeveld, J. Feichter and H. Rodhe, Terrestrial sources and distribution of atmospheric sulphur, *Phil. Trans. R. Soc. Lond. B, 352*, 149-158, 1997.

Liss, P. S. and L. Merlivat, Air-sea gas exchange rates: introduction and synthesis, in: *The role of air-sea exchange in geochemical cycling* (ed. P. Buat-Menard), Reidel, Dordrecht, 1986.

Liss, P. S., A. D. Hatton, G. Malin, P. D. Nightingale and S. M. Turner, Marine sulphur emissions, *Phil. Trans. R. Soc. Lond. B, 352*, 159-169, 1997.

Lohmann, U. and J. Feichter, Impact of sulfate aerosols on albedo and lifetime of clouds: A sensitivity study with the ECHAM4 GCM, *J. Geophys. Res., 102*, 13685-13700, 1997.

Lohmann, U., J. Feichter, J. Penner and R. Leaitch, Indirect effect of sulfate and carbonaceous aerosols: A mechanistic treatment, *J. Geophys. Res., 105*, 12193-12206, 2000.

Martin, G. M., D. W. Johnson and A. Spice, The measurement and parametrisation of effective radius of droplets in warm stratocumulus clouds, *J. Atmos. Sci., 51*, 1823-1842, 1994.

Monteith, J. L. and M. H. Unsworth, *Principles of environmental physics (2^{nd} edition)*, Edward Arnold, London, 1990.

Murphy, D. M., J. R. Anderson, P. K. Quinn, L. M. McInness, F. J. Brechtel, S. M. Kreidenweis, A. M. Middlebrook, M. Pósfai, D. S. Thomson and P. R. Buseck, Influence of sea-salt on aerosol radiative properties in the Southern Ocean marine boundary layer, *Nature, 392*, 62-65, 1998.

Nightingale, P. D., G. Malin, C. S. Law, A. J. Watson, P. S. Liss, M. I. Liddicoat, J. Boutin and R. C. Upstill-Goddard, In situ evaluation of air-sea gas exchange parameterizations using novel conservative and volatile tracers, *Global Biogeochemical Cycles, 14*, 373-387, 2000.

O'Dowd, C. D. and M. H. Smith, Physicochemical properties of aerosol over the Northeast Atlantic: Evidence for wind-speed-related submicron sea-salt aerosol production, *J. Geophys. Res., 98*, 1137-1149, 1993.

O'Dowd, C. D., M. H. Smith, I. E. Consterdine and J. A. Lowe, Marine aerosol, sea-salt, and the marine sulphur cycle: A short review, *Atmos. Environ., 31*, 73-80, 1997.

O'Dowd, C. D., J. A. Lowe and M. H. Smith, Coupling sea-salt and sulphate interactions and its impact on cloud droplet concentration predictions, *Geophys. Res. Let., 26*, 1311-1314, 1999.

Pan, W., M. A. Tatang, G. J. McRae and R. G. Prinn, Uncertainty analysis of indirect radiative forcing by anthropogenic sulfate aerosols, *J. Geophys. Res., 103*, 3815-3823, 1998.

Penkett, S. A., B. M. R. Jones, K. A. Brice and A. E. J. Eggleton, The importance of atmospheric ozone and hydrogen peroxide in oxidising sulphur dioxide in cloud and rainwater, *Atmos. Environ., 13*, 123-137, 1979.

Pham, M., J.-F. Müller, G. P. Brasseur, C. Granier and G. Mégie, A three-dimensional study of the tropospheric sulfur cycle, *J. Geophys. Res., 100*, 26061-26092, 1995.

Pope, V. D., M. L. Gallani, P. R. Rowntree and R. A. Stratton, The impact of new physical parametrizations in the Hadley Centre climate model: HadAM3, *Clim. Dyn., 16*, 123-146, 2000.

Pruppacher, H. R. and J. D. Klett, *Microphysics of clouds and precipitation (2^{nd} edition)*, Kluwer, Dordrecht, 1997.

Quinn, P. K., S. F. Marshall, T. S. Bates, D. S. Covert and V. N. Kapustin, Comparison of measured and calculated aerosol properties relevant to the direct radiative forcing of tropospheric sulfate aerosol on climate, *J. Geophys. Res., 100*, 8977-8991, 1995.

Rasch, P. J., M. C. Barth, J. T. Kiehl, S. E. Schwartz and C. M. Benkovitz, A description of the global sulfur cycle and its controlling processes in the National Center for Atmospheric Research Community Climate Model, version 3, *J. Geophys. Res., 105*, 1367-1385, 2000.

Ravishankara, A. R., Y. Rudich, R. Talukdar and S. B. Barone, Oxidation of atmospheric reduced sulphur compounds: perspective from laboratory studies, *Phil. Trans. Roy. Soc. B, 352*, 171-182, 1997.

Rivera-Carpio, C. A., C. E. Corrigan, T. Novakov, J. E. Penner, C. F. Rogers and J. C. Chow, Derivation of contributions of sulfate and carbonaceous aerosols to cloud condensation nuclei from mass size distributions, *J. Geophys. Res., 101*, 19483-19493, 1996.

Roe, P. L., Some contributions to the modelling of discontinuous flows, in: *Large-Scale Computations in Fluid Mechanics*, Lectures in Applied Mathematics *22*, 163-193, American Mathematical Society, Providence, Rhode Island, 1985.

Roelofs, G.-J., J. Lelieveld and L. Ganzeveld, Simulation of global sulfate distribution and the influence on effective cloud drop radii with a coupled photochemistry-sulfur cycle model, *Tellus B, 50*, 224-242, 1998.

Rogers, R. R. and M. K. Yau, *A short course in cloud physics (3^{rd} edition)*, Pergamon Press, Oxford, 1989.

Rotstayn, L. D., Indirect forcing by anthropogenic aerosols: A global climate model calculation of the effective-radius and cloud-lifetime effects, *J. Geophys. Res., 104*, 9369-9380, 1999.

Seinfeld, J. H. and S. N. Pandis, *Atmospheric chemistry and physics: From air pollution to climate change*, John Wiley, New York, 1998.

Smith, R. N. B., A scheme for predicting layer clouds and their water content in a general circulation model, *Q. J. R. Meteorol. Soc., 116*, 435-460, 1990.

Snider, J. R. and G. Vali, Sulfur dioxide oxidation in winter orographic clouds, *J. Geophys. Res., 99*, 18713-18733, 1994.

Spiro, P. A., D. J. Jacob and J. A. Logan, Global inventory of sulfur emissions with $1° \times 1°$ resolution, *J. Geophys. Res., 97*, 6023-6036, 1992.

Stevenson, D. S., W. J. Collins, C. E. Johnson and R. G. Derwent, The impact of aircraft nitrogen oxide emissions on tropospheric ozone studied with a 3D Lagrangian model including fully diurnal chemistry, *Atmos. Environ., 31*, 1837-1850, 1997.

Tripoli, G. J. and W. R. Cotton, A numerical investigation of several factors contributing to the observed variable intensity of deep convection over South Florida, *J. App. Met., 19*, 1037-1063, 1980.

Twomey, S. A., Pollution and the planetary albedo. *Atmos. Environ., 8*, 1251-1256, 1974.

Twomey, S. A., *Atmospheric Aerosols (Developments in Atmospheric Science, Vol. 7)*, Elsevier, London, 1977.

Wanninkhof, R., Relationship between windspeed and gas exchange over the ocean, *J. Geophys. Res., 97*, 7373-7382, 1992.

Webb, M., C. Senior, S. Bony and J.-J. Morcrette, Combining ERBE and ISCCP data to assess clouds in the Hadley Centre, ECMWF and LMD atmospheric climate models, Submitted to *Clim. Dyn.*, 2000.

Wilson, D. R. and S. P. Ballard, A microphysically based precipitation scheme for the UK Meteorological Office Unified Model, *Q. J. R. Meteorol. Soc., 125*, 1607-1636, 1999.

Table 1. Rate coefficients used in the DMS scheme. T is temperature in K, $[O_2]$ is the the number concentration of oxygen molecules per cm^3.

Rate	Value	Reference
k_1	$1.13 \times 10^{-11}\exp(-254/T)$	*Atkinson et al.* [1997]
k_2	$(1.7 \times 10^{-42}\exp(7810/T)[O_2])/$ $(1 + \{5.5 \times 10^{-31}\exp(7460/T)[O_2]\})$	*Atkinson et al.* [1997]
k_3	$2.6 \times 10^{11}\exp(-9056/T)$	*Ayers et al.* [1996]
k_4	1.0×10^{-14}	*Koga and Tanaka* [1999]
k_5	4.0×10^{-11}	*Koga and Tanaka* [1999]
k_6	$1.1 \times 10^{17}\exp(-12057/T)$	*Ayers et al.* [1996]

Table 2. Comparison of satellite retrievals of cloud droplet effective radius with simulated values from the modern-day run of experiment BOTH (μm).

Region	Han *et al.*	Kawamoto	Model
Global (50°N to 40°S only)	10.7	11.2	10.5
Northern hemisphere	10.0	10.8	9.8
Southern hemisphere	11.4	11.7	11.3
Ocean	11.7	11.8	11.1
Land	7.7	9.5	9.1

Table 3. Pre-industrial to modern-day changes in global annual-mean LWP (gm^{-2}), cloud cover (%), shortwave (SWCF), longwave (LWCF) and net (NCF) cloud forcing (Wm^{-2}).

Experiment	Δ LWP	Δ Cloud	Δ SWCF	Δ LWCF	Δ NCF
1. BOTH	+1.08	+0.20	−2.11	+0.21	-1.89 ± 0.16
2. FIRST	−0.33	−0.01	−1.46	+0.12	-1.34 ± 0.13
3. SECOND	+1.21	+0.33	−0.57	+0.08	-0.49 ± 0.15
4. BOTH-acv	+5.66	+2.03	−4.37	+0.69	-3.68 ± 0.15
5. BOTH-DMS	+0.74	+0.34	−1.50	+0.12	-1.38 ± 0.11
6. BOTH-fix	+1.37	+0.65	−2.47	+0.25	-2.22 ± 0.21

Figure 1

(a) Annual-mean column-integrated SO_4 burden from BOTH simulated using modern sulphur emissions (mg m^{-2}).

(b) As (a) but using pre-industrial emissions.

Figure 2

Comparison between observed SO_4 concentrations and those from the lowest layer of the modern-day simulation of BOTH at the nearest model gridpoint to the observations (μg m^{-3}).
(a) Comparison for the more polluted area covered by the EMEP network.
(b) Comparison with Miami University's data for cleaner 'background' sites — note different scale.

Figure 3

Comparison of modelled cloud droplet effective radius (μm) from the modern-day simulation of BOTH with the satellite retrievals of *Han et al.* [1994] and *Kawamoto* [1999].

Figure 4

(a) Annual-mean change in net cloud forcing (Wm^{-2}) due to the combined indirect effects of anthropogenic sulphate aerosol (experiment BOTH). Negative values are indicated by solid contour lines, positive values by dashed contours.

(b) As (a) but for the first indirect effect only (experiment FIRST).

(c) As (a) but for the second indirect effect only (experiment SECOND).

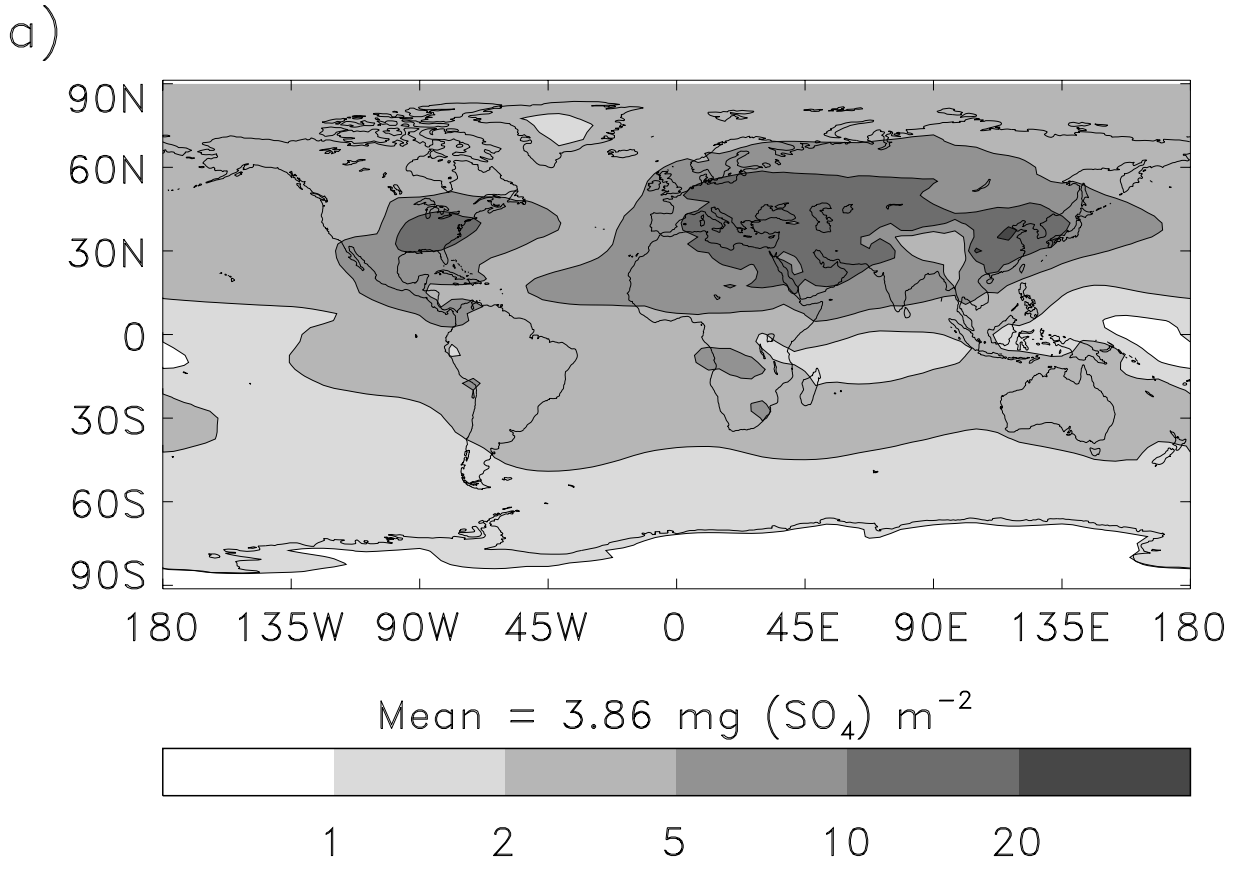
a)
90N
60N
30N
0
30S
60S
90S
180 135W 90W 45W 0 45E 90E 135E 180
Mean = 3.86 mg (SO4) m-2
1 2 5 10 20

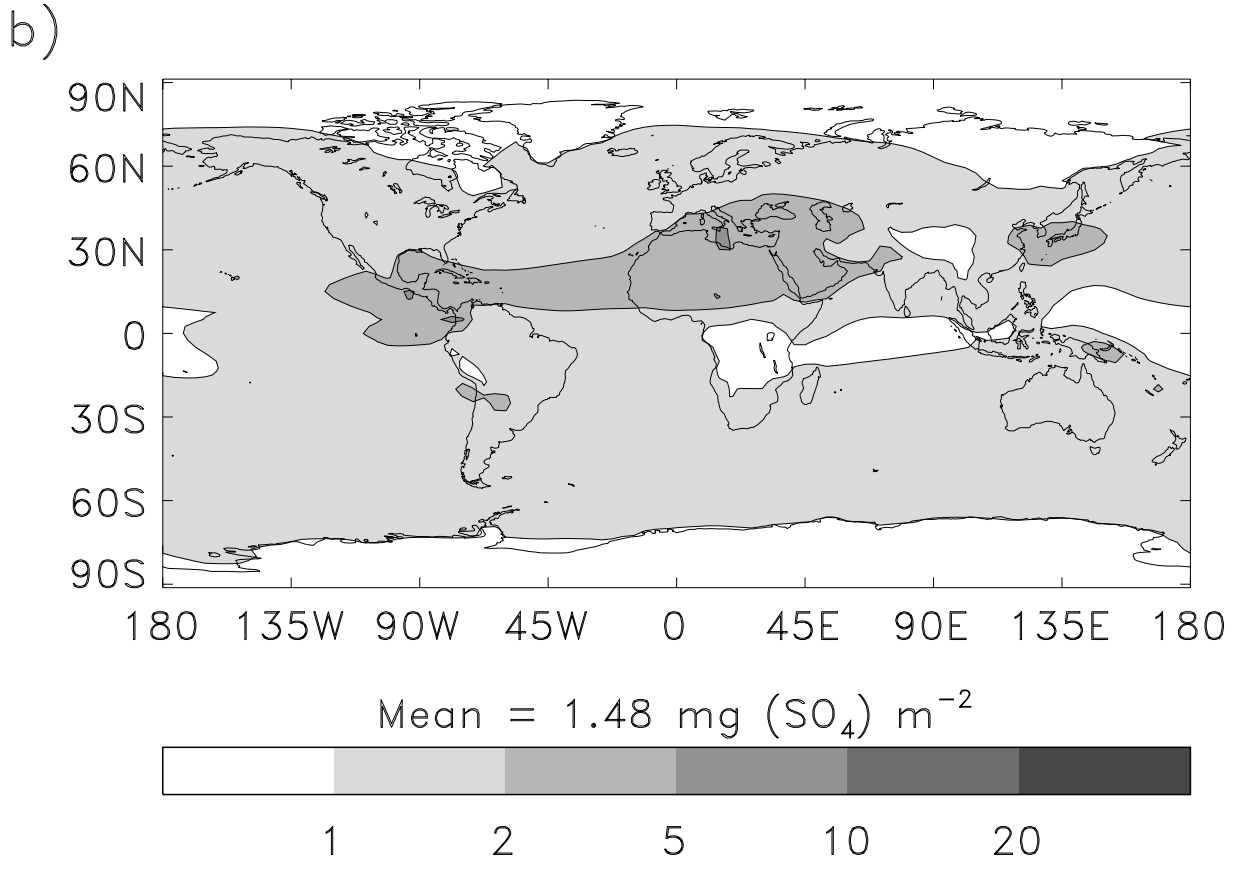
b)
90N
60N
30N
0
30S
60S
90S
180 135W 90W 45W 0 45E 90E 135E 180
Mean = 1.48 mg (SO4) m-2
1 2 5 10 20

a)

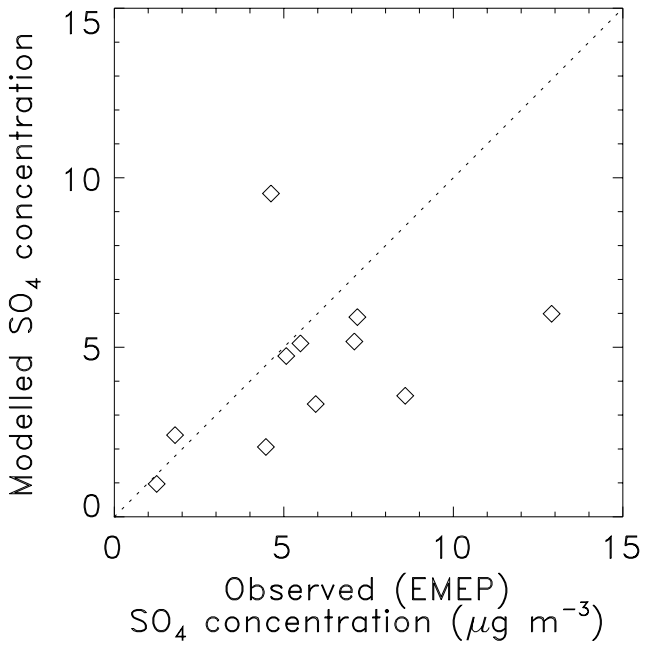
Modelled SO_4 concentration
0
5
10
15
Observed (EMEP)
SO_4 concentration (μg m^{-3})

b)

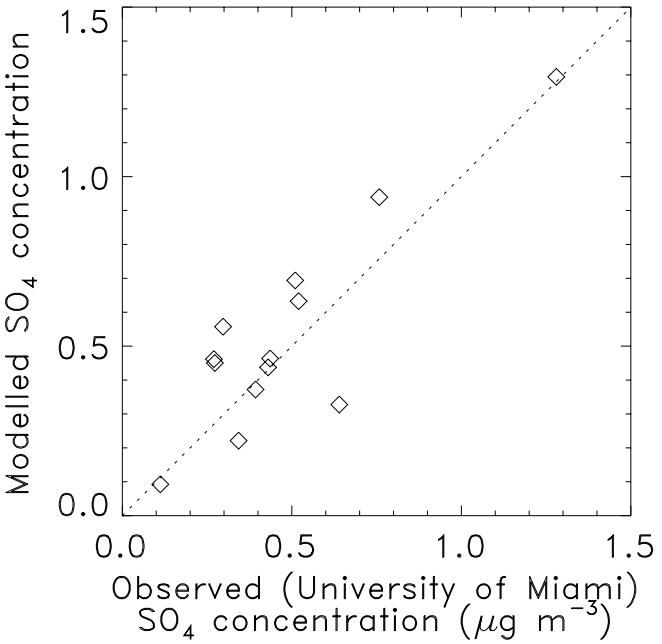
Modelled SO_4 concentration
0.0
0.5
1.0
1.5
Observed (University of Miami)
SO_4 concentration (μg m^{-3})

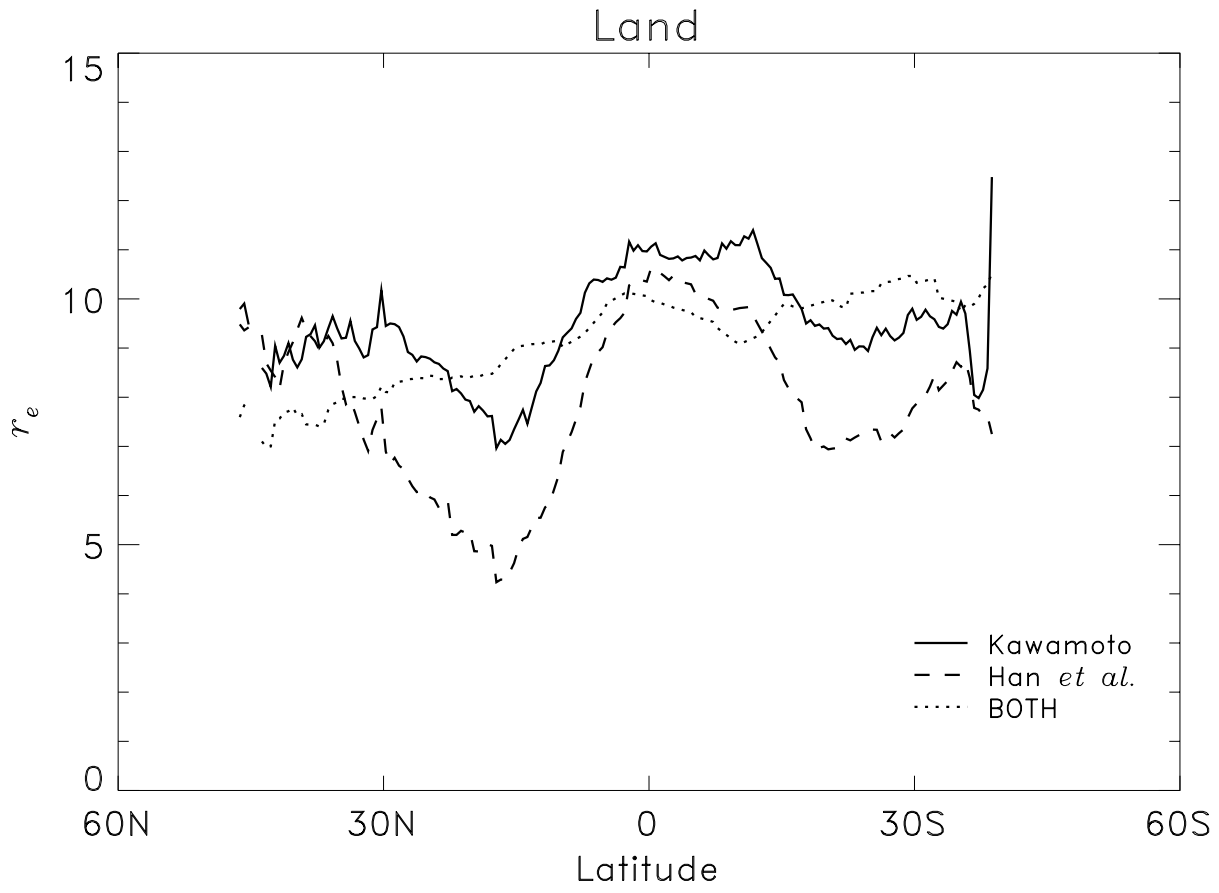
Land
15
10
5
0
r_e
60N
30N
0
30S
60S
Latitude
Kawamoto
Han et al.
BOTH

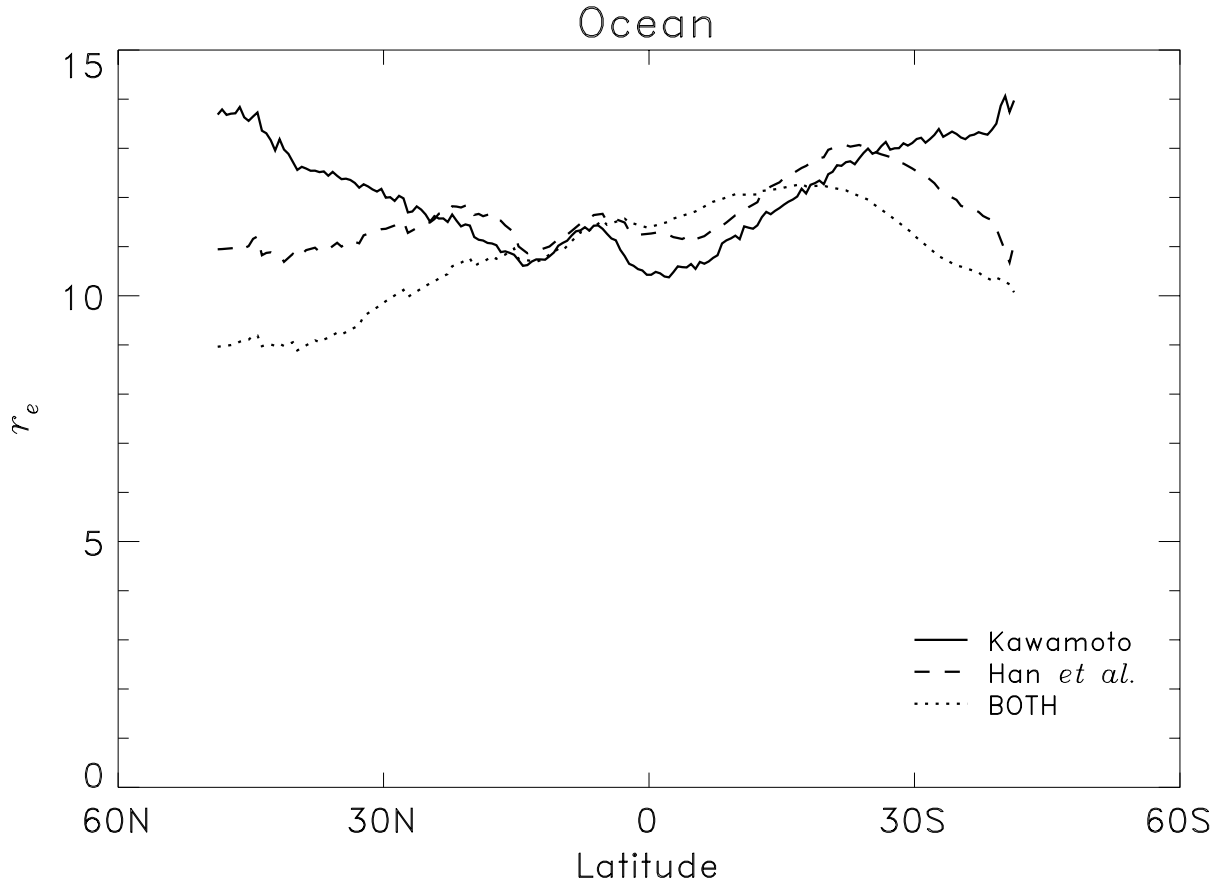
Ocean
15
10
5
0
r_e
60N
30N
0
30S
60S
Latitude
Kawamoto
Han et al.
BOTH

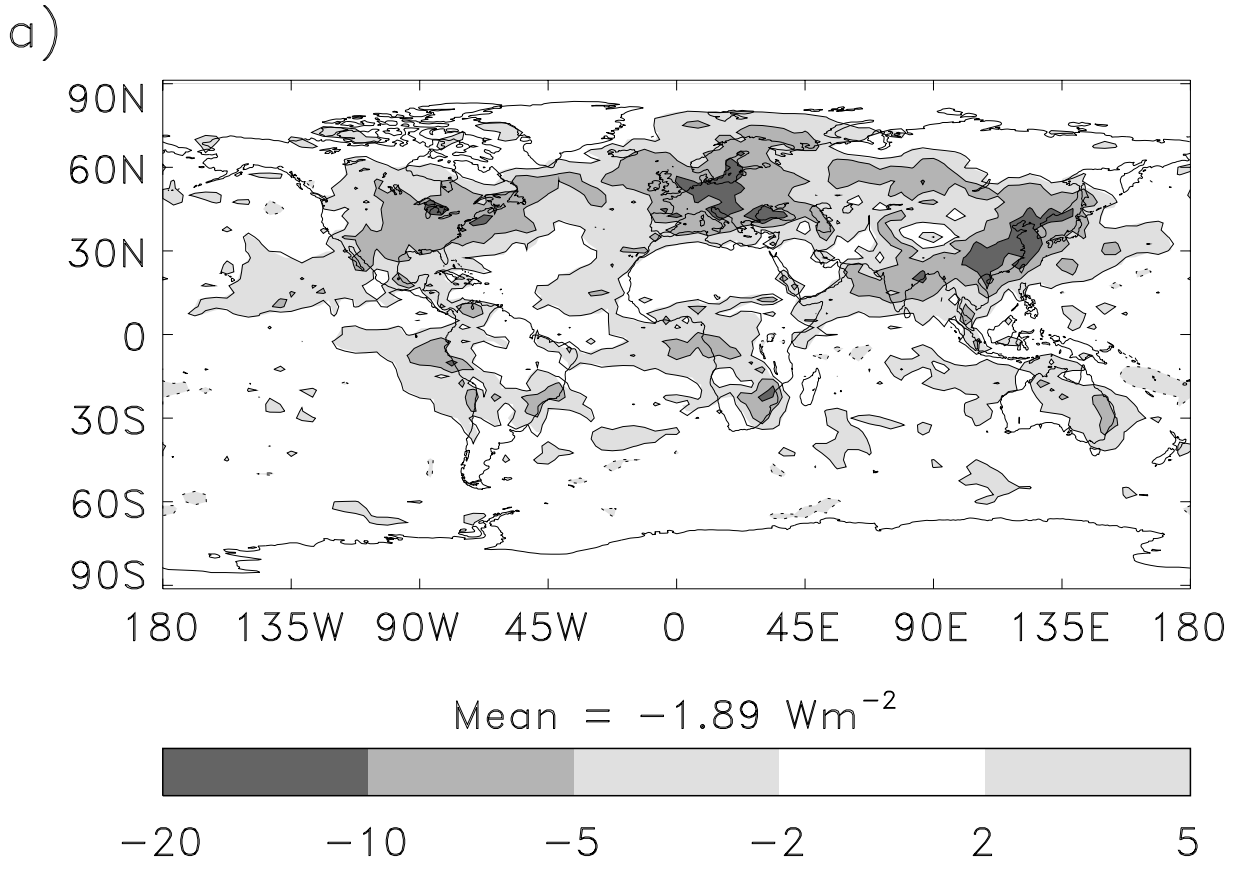
a)
90N
60N
30N
0
30S
60S
90S
180 135W 90W 45W 0 45E 90E 135E 180
Mean = −1.89 Wm^{-2}
−20 −10 −5 −2 2 5

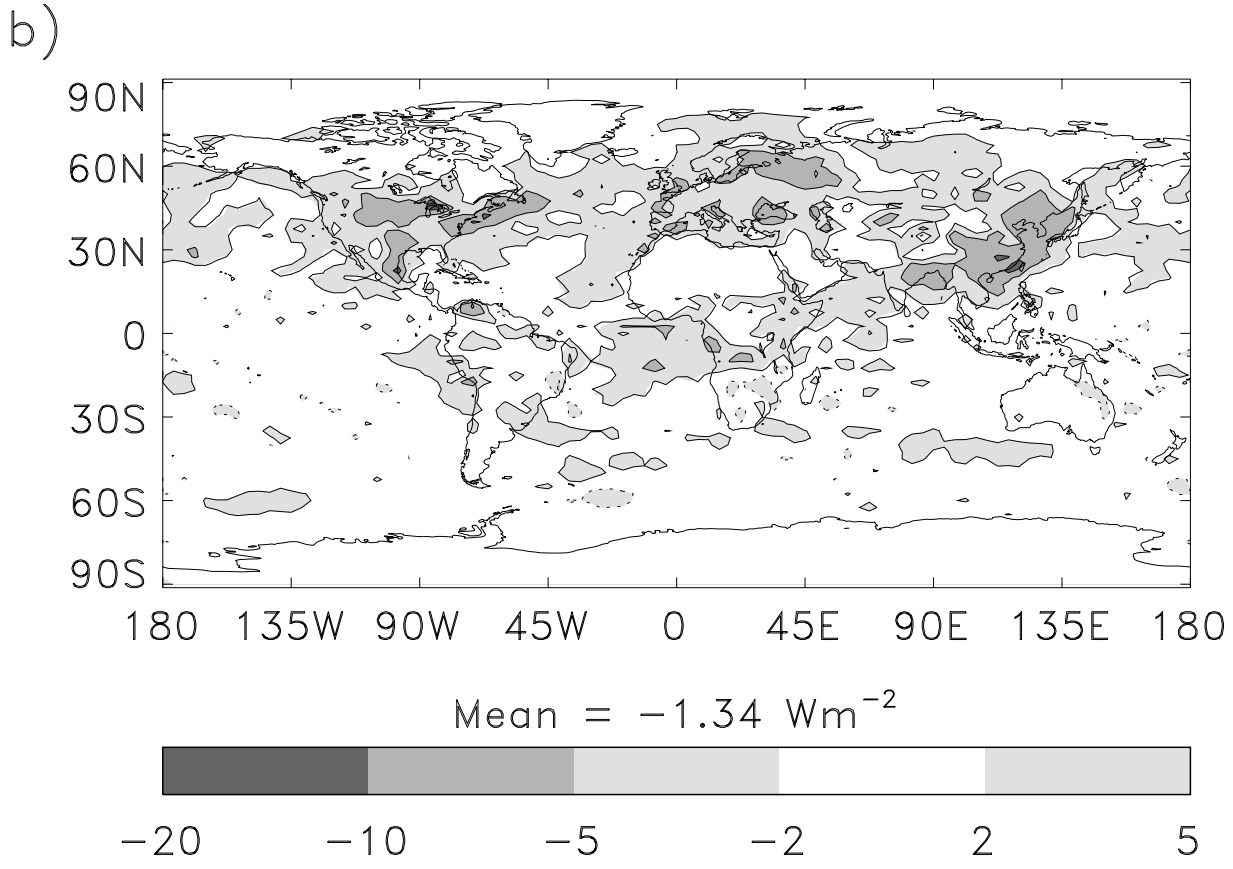
b)
90N
60N
30N
0
30S
60S
90S
180 135W 90W 45W 0 45E 90E 135E 180
Mean = −1.34 Wm^{-2}
−20 −10 −5 −2 2 5

c)

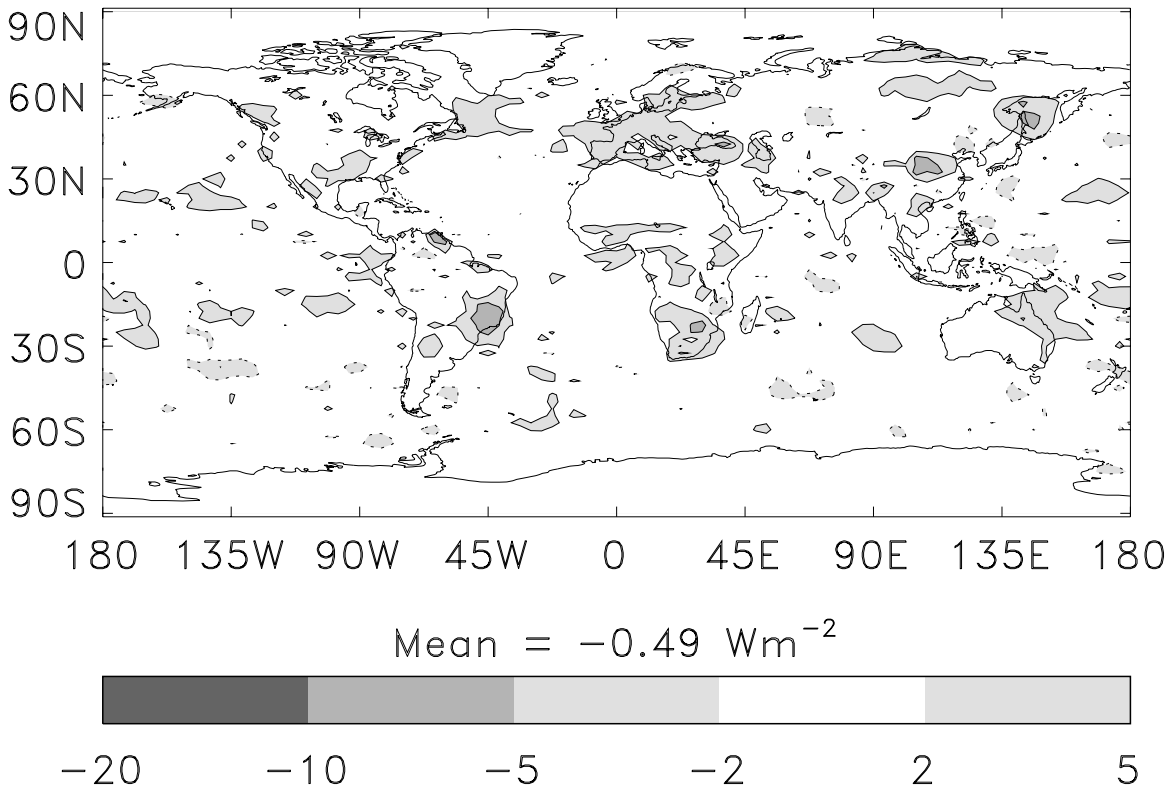
90N
60N
30N
0
30S
60S
90S
180 135W 90W 45W 0 45E 90E 135E 180
Mean = −0.49 Wm^{-2}
−20 −10 −5 −2 2 5